



1 **Aerosol optical properties and instantaneous radiative forcing based on**
2 **high temporospatial resolution CARSNET ground-based measurements**
3 **over eastern China**

4 Huizheng Che^{1*}, Bing Qi², Hujia Zhao¹, Xiangao Xia^{3,4}, Philippe Goloub⁵, Oleg Dubovik⁵,
5 Victor Estelles⁶, Emilio Cuevas-Agulló⁷, Luc Blarel³, Yunfei Wu⁸, Jun Zhu⁹, Rongguang Du²,
6 Yaqiang WANG¹, Hong Wang¹, Ke Gui¹, Jie Yu¹, Yu Zheng⁹, Tianze Sun¹, Quanliang Chen¹⁰,
7 Guangyu Shi¹¹, Xiaoye Zhang^{1*}

8 1 State Key Laboratory of Severe Weather (LASW) and Institute of Atmospheric
9 Composition, Chinese Academy of Meteorological Sciences, CMA, Beijing, 100081,
10 China

11 2 Hangzhou Meteorological Bureau, Hangzhou, 310051, China

12 3 Laboratory for Middle Atmosphere and Global Environment Observation (LAGEO),
13 Institute of Atmospheric Physics, Chinese Academy of Sciences, Beijing, 100029, China

14 4 School of Geoscience University of Chinese Academy of Science, Beijing, 100049, China

15 5 Laboratoire d'Optique Atmosphérique, Université des Sciences et Technologies de Lille,
16 59655, Villeneuve d'Ascq, France

17 6 Dept. Física de la Terra i Termodinàmica, Universitat de València, C/ Dr. Moliner 50,
18 46100 Burjassot, Spain

19 7 Centro de Investigación Atmosférica de Izaña, AEMET, 38001 Santa Cruz de Tenerife ,
20 Spain

21 8 Key Laboratory of Regional Climate-Environment for Temperate East Asia, Institute of
22 Atmospheric Physics, Chinese Academy of Sciences, Beijing 100029, China

23 9 Collaborative Innovation Center on Forecast and Evaluation of Meteorological Disasters,
24 Nanjing University of Information Science & Technology, Nanjing 210044, China

25 10 Plateau Atmospheric and Environment Key Laboratory of Sichuan Province, College of
26 Atmospheric Sciences, Chengdu University of Information Technology, Chengdu, 610225,
27 China

28 11 State Key Laboratory of Numerical Modeling for Atmospheric Sciences and Geophysical
29 Fluid Dynamics (LASG), Institute of Atmospheric Physics, Chinese Academy of Sciences,
30 Beijing, 100029, China

31 Corresponding author: chehz@camsma.cn & xiaoye@camsma.cn

32



33 **Abstract**

34 Variations in the optical properties of aerosols and their radiative forcing were investigated
35 based on long-term synchronous observations made at three-minute intervals from 2011 to
36 2015 over seven adjacent CARSNET (China Aerosol Remote Sensing NETwork) urban
37 (Hangzhou), suburban (Xiaoshan, Fuyang, LinAn, Tonglu, Jiande) and rural (ChunAn) stations
38 in the Yangtze River Delta region, eastern China. The aerosol optical depth (AOD) varied from
39 0.68 to 0.76, with two peaks in June and September, and decreased from the eastern coast to
40 western inland areas. The ratio of the AOD of fine-mode particles to the total AOD was >0.90
41 and the extinction Angström exponent was >1.20 throughout the year at all seven sites. The
42 Moderate Resolution Imaging Spectroradiometer (MODIS) C6 retrieval AOD was validated by
43 comparison with ground-based observations. The correlation coefficients (R^2) between the
44 MODIS C6 AOD data and the values measured on the ground were ~0.73–0.89. The
45 single-scattering albedo varied from 0.91 to 0.94, indicating that scattering aerosol particles
46 are dominant in this region. The real parts of the refractive index were ~1.41–1.43, with no
47 significant difference among the seven urban, suburban and rural sites. Large imaginary parts
48 of the refractive index were seen in August at all urban, suburban and rural sites. The
49 fine-mode radii in the Yangtze River Delta region were ~0.2–0.3 μm with a volume of 0.10–
50 0.12 μm^3 and the coarse-mode radii were ~2.0 μm with a volume close to 0.07 μm^3 . The
51 fine-mode aerosols were obviously larger in June and September than in other months at
52 almost the sites. The absorption AOD was low in the winter. The absorption Angström
53 exponent and the extinction Angström exponent were used to classify the different types of
54 aerosol and the components of mixtures. The aerosols caused negative radiative forcing both
55 at the Earth's surface and at the top of the atmosphere all year round in the Yangtze River
56 Delta region of eastern China.



57 1. Introduction

58 Aerosols have important effects on the Earth's climate at both global and regional scales,
59 although there are still great uncertainties in assessing their impact (Hansen et al. 2000;
60 Solomon et al., 2007; Schwartz and Andreae, 1996). Aerosols affect not only the radiative
61 balance of the Earth–atmosphere system by directly scattering and absorbing solar radiation
62 (Charlson et al., 1992; Ackerman and Toon, 1981), but also indirectly affect the climate through
63 aerosol – cloud interactions (Twomey et al., 1984; Albrecht et al., 1989; Li et al., 2016).

64 The optical properties of aerosols influence the aerosol radiative balance and can be
65 used to predict and assess global and regional changes in the Earth's climate (Eck et al., 2005;
66 Myhre et al., 2009; IPCC, 2013; Panicker et al., 2013). Long-term, ground-based observations
67 are crucial to our understanding of the global and regional variations in the optical properties of
68 aerosols and their effects on the Earth's climate (Holben et al., 2001; Kaufman et al., 2002;
69 Sanap and Pandithurai, 2014; Li et al., 2016). Ground-based monitoring networks have been
70 established worldwide—for instance, AERONET (Holben et al., 1998; Goloub et al., 2007),
71 SKYNET (Takamura et al., 2004), EARLINET (Pappalardo et al., 2014) and the GAW-PFR
72 Network (Wehrli, 2002; Estelles et al., 2012), which includes several automated sites in China.
73 CARSNET (the China Aerosol Remote Sensing NETwork) (Che et al., 2009a, 2015b) and
74 CSHNET (the Chinese Sun Hazemeter Network) were established to obtain data on aerosol
75 optical characteristics in China (Xin et al., 2007).

76 Most of the ground-based studies of the optical properties of aerosols in China have been
77 concentrated in urban regions undergoing rapid economic development, which have high
78 aerosol loadings and serious environmental problems (Cheng et al., 2015; Pan et al., 2010;
79 Xia et al., 2013; Wang et al., 2015; Che et al., 2015a). Analyses of the aerosol optical depth
80 (AOD), the types of aerosol present and the classification of ambient aerosol populations
81 based on their size and absorption properties (Giles et al., 2011) are needed to understand
82 their effects on the Earth's climate and environment (Che et al., 2009b; Wang et al., 2010; Zhu
83 et al., 2014).



84 The Yangtze River Delta (YRD) region in eastern China has undergone rapid economic
85 growth and has high emissions of aerosols (Fu et al., 2008; Zhang et al., 2009). There have
86 been many studies of the optical properties of aerosols in eastern China and these are
87 important in our understanding of both the local air quality and regional climate change (Duan
88 and Mao, 2007; Pan et al., 2010; Ding et al., 2016). Basic investigations of the variation in the
89 optical characteristics of aerosols over the YRD region have been carried out at Nanjing, Hefei,
90 Shanghai, Shouxian and Taihu (Zhuang et al. 2014; Li et al., 2015; Wang et al., 2015; He et al.,
91 2012; Lee et al., 2010; Cheng et al., 2015; Xia et al., 2007). These studies in the YRD region
92 have mostly been single-site and/or short-period investigations. The study sites are ~100 km
93 apart from each other, which makes high spatial resolution satellite and modeling validations
94 difficult. Thus there is still a lack of long-term, continuous and synchronous observations of the
95 optical characteristics of aerosols, especially over adjacent urban, suburban and rural areas in
96 the YRD region.

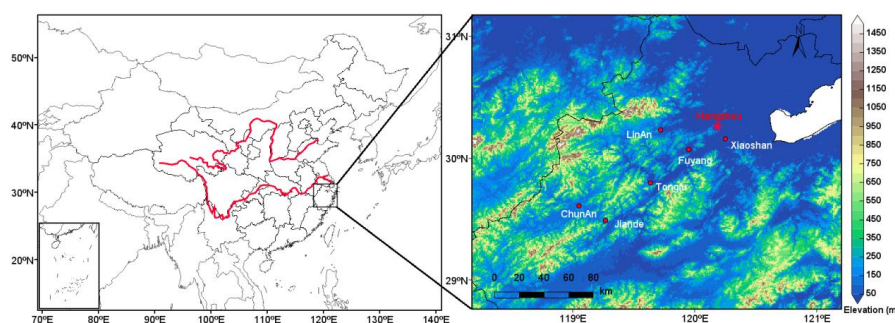
97 High-frequency ground-based observations of the variations in the optical characteristics
98 of aerosols are necessary to our understanding of the processes involved in air pollution (e.g.
99 the source, transport and diurnal variations of the pollution) and their effect on the regional
100 climate. Ground-based observations are also important in the validation and improvement of
101 satellite retrieval data (Holben et al., 2017; Xie et al., 2011). A high density of ground-based
102 sun- and sky-scanning spectral radiometers within a local or meso-scale region is required to
103 capture small-scale variations in aerosols for the accurate validation of satellite observations
104 and to compare in situ versus remote sensing observations (Xiao et al., 2016; Holben et al.,
105 2017). The MODIS (Moderate Resolution Imaging Spectroradiometer) retrieval AOD has a
106 high accuracy with a wide spectral coverage (Tanré et al., 1997; Kaufman, et al. 1997) and the
107 algorithm has been validated and improved based on AERONET data (Chu et al., 2002;
108 Ichoku et al., 2002; Remer et al., 2005; Levy et al., 2010;). Levy et al. (2013) refined the
109 MODIS Collection 6 (C6) aerosol retrieval process to provide better AOD retrievals. Some
110 validations of satellite aerosol retrievals have been carried out in China with ground-based
111 observations from CSHNET (Li, et al., 2007; Wang, et al., 2007; Xin, et al., 2007) and
112 CARSNET (Che et al., 2009a, Che et al., 2011a; Tao et al., 2015).



113 We investigated the variation in the optical properties of aerosols and aerosol radiative
114 forcing (ARF) using three-minute intervals of sun photometer measurements from 2011 to
115 2015 at seven adjacent CARSNET (~10–40 km) urban, suburban and rural sites over eastern
116 China. The aims of this study were: (1) to investigate the synchronous variations and
117 differences in the optical properties of aerosols over urban, suburban and rural areas of the
118 YRD megacity, eastern China; (2) to analyze the type and dominant distribution pattern of
119 aerosols in the YRD via the extinction and absorption properties of aerosols; (3) to understand
120 the difference in the ARF calculated from ground-based measurements of the optical
121 properties of aerosols over urban, suburban and rural areas in eastern China; and (4) to
122 evaluate the MODIS AOD retrieval data using the CARSNET AOD for the YRD. The results of
123 this study will help the satellite and modeling communities to improve future aerosol retrieval
124 data and simulations.

125 2. Site descriptions, measurements and data

126 Fig. 1 shows the geographical locations of the seven CARSNET sites in the YRD; these
127 locations are described in Table 1.



128
129 Fig. 1. Geographical location and elevation map for the seven CARSNET sites in the YRD.

130 The rural site of ChunAn can be regarded as a representative background location
131 unaffected by local and regional pollution. The site has a small population and a good
132 ecological environment, although there is some agricultural activity and burning of biomass
133 from crop residues. Hangzhou is a densely populated urban site with a large volume of



134 vehicular traffic and is therefore more affected by anthropogenic activity. LinAn, Fuyang,
135 Jiande, Xiaoshan Tonglu and Xiaoshan are suburban sites and are all affected by both
136 anthropogenic activity and pollution from industrial and agricultural production.

137 CE-318 sun photometers (Cimel Electronique, Paris, France) were installed at these
138 seven sites in the YRD from 2011 to 2015. The instruments were standardized and calibrated
139 annually according to the protocols reported by Che et al. (2009a). The instruments in this
140 study were made inter-comparison calibration by the CARSNET reference instruments, which
141 were periodically calibrated at Izaña in Spain. The cloud-screened AOD at different
142 wavelengths was obtained using ASTPwin software (Cimel Electronique) (Smirnov et al.,
143 2000). Instantaneous direct data for the AOD were selected at least ten times each day at a
144 temporal resolution of about three minutes and the corresponding values of Angström
145 exponent (α) were calculated by instantaneous AOD values at 440 and 870 nm.

146 The aerosol optical properties—including the single-scattering albedo (SSA), the complex
147 refractive index, the volume size distribution, the absorption AOD (AAOD), the absorption
148 Angström exponent (AAE) and the fraction of spherical particles—were retrieved from the
149 almucantar irradiance measurements according to the methods of Dubovik and King (2000)
150 and Dubovik et al. (2002, 2006). The SSA was retrieved using only $AOD_{440nm} > 0.40$
151 measurements to avoid the large uncertainties inherent in a low AOD. The complex refractive
152 index was also retrieved by sky irradiance measurements in the range 1.33–1.60 for the real
153 part and in the range 0.0005–0.50 for the imaginary part (Dubovik and King, 2000; Che et al.,
154 2015b). In the volume size distribution, the radius range is selected from 0.05–15 μ m. The
155 AAOD and the AAE were calculated as described in equations (1) and (2):

$$156 \quad AAOD(\lambda) = [1 - SSA(\lambda)] \times EAOD(\lambda) \quad (1)$$

$$157 \quad AAE = -d\ln[AAOD(\lambda)]/d\ln(\lambda) \quad (2)$$

158 The ARF data were calculated by the radiative transfer module used by the AERONET
159 inversion (García et al., 2012). The broadband fluxes from 0.20 to 4.0 μ m were calculated
160 according to the radiative transfer model GAME (Global Atmospheric ModEl) (Dubuisson et al.,



161 1996, 2006; Roger et al., 2006).

162 The MODIS C6 aerosol optical thickness products refined by Levy et al. (2013) were used
163 to compare the MODIS AOD retrievals with our ground-based observations. The MODIS C6
164 AOD retrievals were formed into a merged dataset combining the Deep Blue and Dark Target
165 methods. This version of MODIS includes some important changes from earlier
166 versions—such as the central wavelength assumptions, Rayleigh scattering and the gas
167 absorption performance (Levy et al., 2013)—and improvements in the radiometric calibration
168 (Lyapustin et al., 2014). All cloud- and snow-free land surfaces have been expanded in the
169 MODIS C6 aerosol products (Hsu et al., 2013). The AOD data from Terra-MODIS were
170 validated by matching the CARSNET AODs within 30 minutes of the MODIS overpass within
171 the 3×3 pixels surrounding the CARSNET site. The AOD at 550 nm was interpolated between
172 two wavelengths of the ground-based AOD measurements at 440 and 675 nm.

173 3. Results and discussion

174 3.1 Aerosol optical depth and Angström exponent

175 The AOD over the seven urban, suburban and rural sites in this study varied from 0.68 to
176 0.76 (Table 1). The annual values of the AOD at Hangzhou, Xiaoshan, Fuyang, LinAn, Tonglu,
177 Jiande and ChunAn were about 0.76 ± 0.42 , 0.76 ± 0.43 , 0.76 ± 0.45 , 0.73 ± 0.44 , 0.71 ± 0.41 ,
178 0.73 ± 0.40 and 0.68 ± 0.38 , respectively, which suggests that aerosol loading is at a high level at
179 all seven urban, suburban and rural sites in the YRD. This suggests that aerosol pollution is on
180 the regional rather than the local scale in the YRD region. The AOD at the urban site of
181 Hangzhou was the highest of all the study sites as a result of high local anthropogenic activity
182 in this urban area compared with the other suburban and rural sites. The AOD at the rural site
183 of ChunAn was lower than at the urban and suburban sites due to lower levels of
184 anthropogenic activity. The AOD decreased from the eastern coast to the inland areas towards
185 the west (from $\sim 0.76\pm 0.42$ at Hangzhou to $\sim 0.68\pm 0.38$ at ChunAn). This is due to the high
186 aerosol loading from economic development and anthropogenic influences. There is more
187 industrial activity and high resident density in the eastern part of the Hangzhou metropolis



188 region, resulting in higher aerosol emissions. The AOD in Hangzhou in urban eastern China
 189 was similar to that in Shenyang (0.75) in urban northeast China (Zhao et al., 2013), and in
 190 Beijing (0.76) and Tianjin (0.74) in urban north China (Che et al., 2015b), indicating that
 191 aerosol pollution is both common and at a similar level throughout most urban areas of China.
 192 The AOD values at the urban and suburban sites of Hangzhou were slightly higher than at
 193 Pudong (0.70) and Hefei (0.69), other urban areas in eastern China, suggesting that higher
 194 aerosol loadings were emitted here (He et al., 2012; Liu et al., 2017). However, the AOD at all
 195 seven sites was lower than that obtained at Wuhan (1.05), Nanjing (0.88), Dongtan (0.85),
 196 Taihu (0.77) and Xuzhou (0.92) in previous studies in eastern China (Wang et al., 2015; Li et
 197 al., 2015; Pan et al., 2010; Xia et al., 2007; Wu et al., 2016). This indicates that the aerosol
 198 loading caused by anthropogenic activities is very high in both urban and suburban areas in
 199 eastern China. The site at LinAn is regarded as the regional background site in eastern China
 200 and is representative of the background atmospheric characteristics of this region (Che et al.,
 201 2009c). The average AOD at LinAn was about 0.73 ± 0.44 , which is higher than that at the other
 202 regional background stations of China, such as Longfengshan (0.35; northeastern China), Mt
 203 Waliguan (0.14, inland Asia), Xinglong (0.28, northern China), Akedala (0.20, northwestern
 204 China) and Shangri-La (0.11, southwestern China) (Wang et al., 2010; Che et al., 2011; Zhu et
 205 al., 2014; Che et al., 2015b). The aerosol loading in eastern China (especially in the YRD
 206 region) is at least twice as high as in other regions of China.

207 Table 1. Geographical location and annual mean optical parameters of aerosols at the seven
 208 observation sites in the YRD.

	Hangzhou	Xiaoshan	Fuyang	LinAn	Tonglu	Jiande	ChunAn
Site type	Urban	Suburban	Suburban	Suburban	Suburban	Suburban	Rural
Longitude (° E)	120.19	120.25	119.95	119.72	119.64	119.27	119.05
Latitude (° N)	30.26	30.16	30.07	30.23	29.80	29.49	29.61
Altitude (m)	41.9	14.0	17.0	139	46.1	88.9	171.4
^a N_{day}	485	180	217	562	498	480	439
^b $N_{\text{inst.}}$	2052	752	906	2410	2255	1952	1731
^c AOD	0.76 ± 0.42	0.76 ± 0.43	0.76 ± 0.45	0.73 ± 0.44	0.71 ± 0.41	0.73 ± 0.40	0.68 ± 0.38
^c AOD _{fine}	0.68 ± 0.42	0.69 ± 0.41	0.69 ± 0.44	0.66 ± 0.43	0.64 ± 0.41	0.66 ± 0.40	0.61 ± 0.38
^c AOD _{coarse}	0.08 ± 0.06	0.07 ± 0.06	0.07 ± 0.06	0.07 ± 0.07	0.07 ± 0.06	0.07 ± 0.07	0.06 ± 0.05
^d EAE	1.29 ± 0.26	1.37 ± 0.24	1.32 ± 0.24	1.29 ± 0.27	1.30 ± 0.26	1.32 ± 0.28	1.22 ± 0.25



^c SSA	0.91±0.06	0.93±0.04	0.94±0.04	0.93±0.05	0.92±0.04	0.92±0.05	0.94±0.03
^c SSA _{fine}	0.93±0.05	0.95±0.04	0.95±0.04	0.94±0.04	0.94±0.04	0.94±0.05	0.95±0.03
^c SSA _{coarse}	0.82±0.09	0.83±0.08	0.84±0.08	0.81±0.08	0.81±0.08	0.82±0.09	0.81±0.07
^c Real	1.43±0.07	1.41±0.06	1.41±0.06	1.42±0.06	1.43±0.06	1.41±0.05	1.41±0.05
^c Imaginary	0.011±0.010	0.008±0.006	0.007±0.006	0.009±0.007	0.009±0.007	0.010±0.009	0.007±0.004
^c AAOD	0.06±0.05	0.05±0.04	0.04±0.04	0.05±0.04	0.05±0.04	0.06±0.04	0.04±0.03
^d AAE	1.13±0.46	0.88±0.42	0.85±0.43	0.98±0.35	1.11±0.49	1.16±0.44	0.93±0.31
^c Rmeas _t (μm)	0.70±0.34	0.65±0.31	0.66±0.33	0.66±0.33	0.65±0.33	0.62±0.24	0.65±0.30
^c Rmea _{fine} (μm)	0.18±0.05	0.18±0.04	0.19±0.05	0.19±0.05	0.19±0.05	0.19±0.05	0.20±0.05
^c Rmea _{coarse} (μm)	2.67±0.47	2.73±0.42	2.75±0.45	2.71±0.52	2.66±0.48	2.63±0.47	2.74±0.49
^c Reff (μm)	0.30±0.10	0.29±0.09	0.30±0.09	0.29±0.10	0.29±0.10	0.29±0.09	0.30±0.10
^c Reff _{fine} (μm)	0.16±0.04	0.16±0.03	0.17±0.04	0.16±0.04	0.16±0.04	0.17±0.04	0.17±0.04
^c Reff _{coarse} (μm)	2.21±0.40	2.26±0.35	2.30±0.39	2.24±0.44	2.19±0.41	2.16±0.39	2.27±0.42
^c Volume (μm ³)	0.19±0.09	0.19±0.09	0.19±0.09	0.18±0.09	0.17±0.09	0.18±0.09	0.17±0.07
^c Volume _{fine} (μm ³)	0.10±0.06	0.11±0.06	0.11±0.07	0.10±0.06	0.10±0.06	0.10±0.06	0.10±0.06
^c Volume _{coarse} (μm ³)	0.09±0.06	0.08±0.05	0.08±0.06	0.08±0.05	0.08±0.06	0.08±0.07	0.07±0.05
^c ARF-BOT (W/m ²)	-93±44	-84±41	-80±40	-81±39	-79±39	-82±40	-74±34
^c ARF-TOA (W/m ²)	-35±20	-36±21	-37±21	-36±21	-35±20	-35±21	-40±19

209 ^a Number of available observation days.

210 ^b Number of instantaneous observations.

211 ^c Optical parameters at a wavelength of 440 nm.

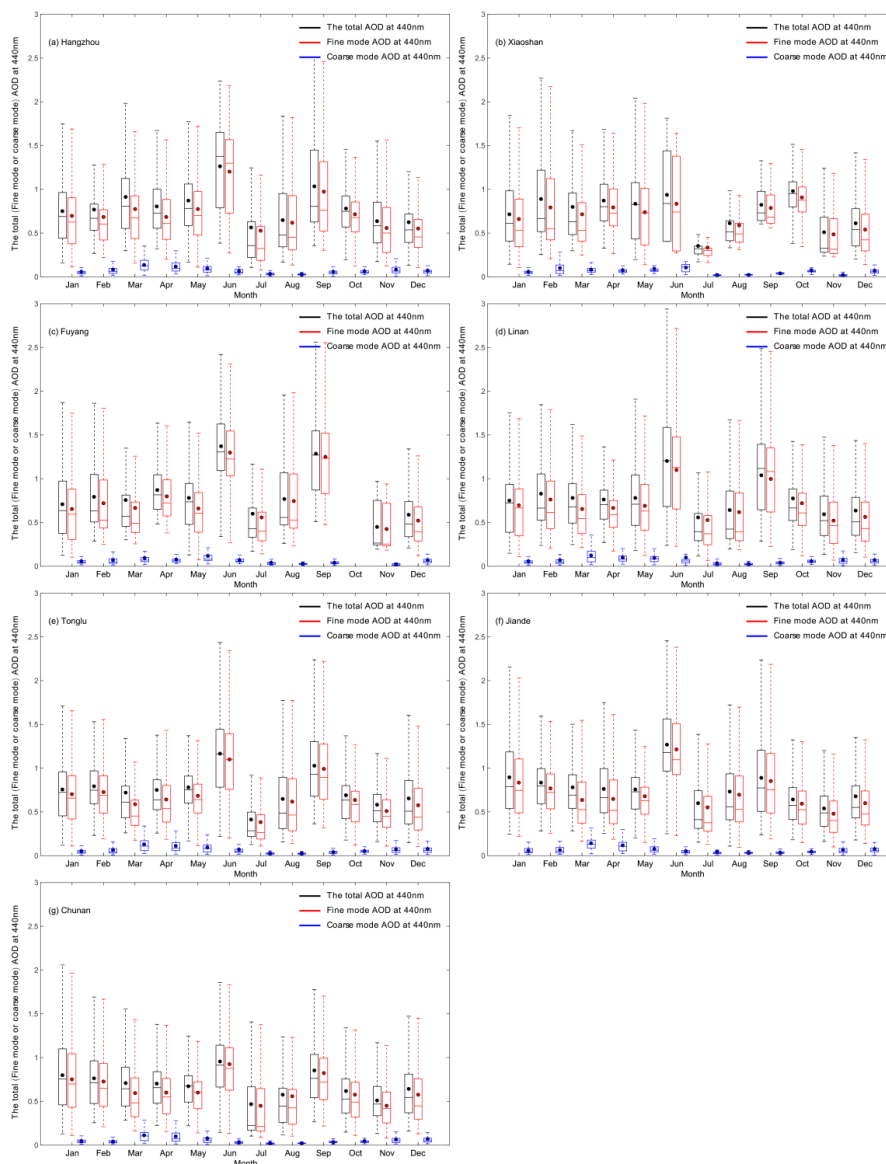
212 ^d Angström exponents between 440 and 870 nm.

213

214 Ding et al. (2013a, b) showed that plumes from agricultural burning in June may
 215 significantly and seriously affect the radiation balance and air quality of the YRD region. In this
 216 study, the monthly averaged AODs at most sites showed two peaks in June and September
 217 (Fig. 2) with values of $\sim 1.26 \pm 0.50$ and $\sim 1.03 \pm 0.57$, respectively. This may be attributed to the
 218 accumulation of fine-mode particles via hygroscopic growth in the summer season and the
 219 burning of crop residue biomass under a continental high-pressure system with good
 220 atmospheric stability and frequent temperature inversions. These conditions lead to the poor
 221 diffusion of pollutants (Xia et al., 2007).



222 The annual fine-mode AOD values at Hangzhou, Xiaoshan, Fuyang, LinAn, Tonglu,
223 Jiande and ChunAn were about 0.68 ± 0.42 , 0.69 ± 0.41 , 0.69 ± 0.44 , 0.66 ± 0.43 , 0.64 ± 0.41 ,
224 0.66 ± 0.40 and 0.61 ± 0.38 , respectively (Fig. 2). The seasonal variation in the AOD was similar
225 to the total AOD at these urban, suburban and rural sites. The ratio AOD_f/AOD_t consistently
226 exceeded 0.90 at all sites, which indicates that fine-mode particles make a major contribution
227 to the total AOD in the YRD. The annual coarse-mode AOD values at Hangzhou, Xiaoshan,
228 Fuyang, LinAn, Tonglu, Jiande and ChunAn were between about 0.06 and 0.08. The ratio
229 AOD_c/AOD_t was about 0.10, which indicates that about 10% of the contribution to the AOD in
230 the YRD region is from coarse particles. The variation in the coarse-mode AOD (Fig. 2) also
231 showed a significant increase in March at all seven sites of about 0.14 ± 0.08 , 0.08 ± 0.04 ,
232 0.09 ± 0.09 , 0.13 ± 0.11 , 0.13 ± 0.11 , 0.14 ± 0.08 and 0.11 ± 0.07 at Hangzhou, Xiaoshan, Fuyang,
233 LinAn, Tonglu, Jiande and ChunAn, respectively. This was mainly caused by dust episodes
234 from north/northwest China, which contributed to the optical properties of aerosols in this
235 region (Zhang et al., 2012).



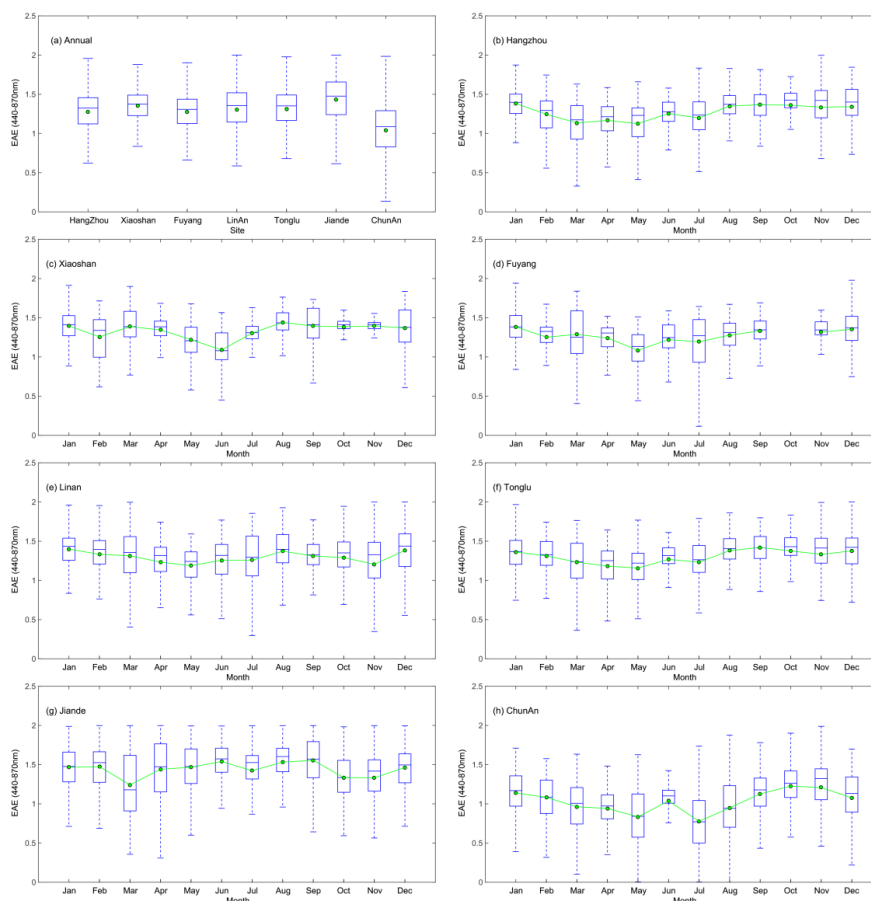
236

237 Fig. 2. Variation in the total, fine- and coarse-mode AOD_{440 nm} over (a) Hangzhou,
238 (c) Fuyang, (d) LinAn, (e) Tonglu, (f) Jiande and (g) ChunAn. The boxes represent the 25th to
239 75th percentile distribution, while the dots and solid lines within each box represent the mean
240 and median, respectively.

241 Figure 3 shows that the annual extinction Angström exponent (EAE) at Hangzhou,



242 Xiaoshan, Fuyang, LinAn, Tonglu, Jiande and ChunAn was about 1.29 ± 0.26 , 1.37 ± 0.24 ,
243 1.32 ± 0.24 , 1.29 ± 0.27 , 1.30 ± 0.26 , 1.32 ± 0.28 and 1.22 ± 0.25 , respectively. Values of EAE > 1.20
244 were found in all months throughout the year, indicating that small particle size distributions
245 were favored in the YRD region. The monthly average value of the EAE in Hangzhou was
246 higher in January ($\sim 1.40 \pm 0.23$) and September ($\sim 1.43 \pm 0.24$). This indicated the dominance of
247 small particles from anthropogenic emissions and agricultural activity in autumn and winter
248 (Tan et al., 2009). The EAE was lower in March ($\sim 1.16 \pm 0.24$) and April ($\sim 1.13 \pm 0.22$), which
249 reflects the effect of mineral dust aerosols (Gong et al., 2003). However, this effect is not as
250 obvious in the YRD region as other regions in north or northeast China.



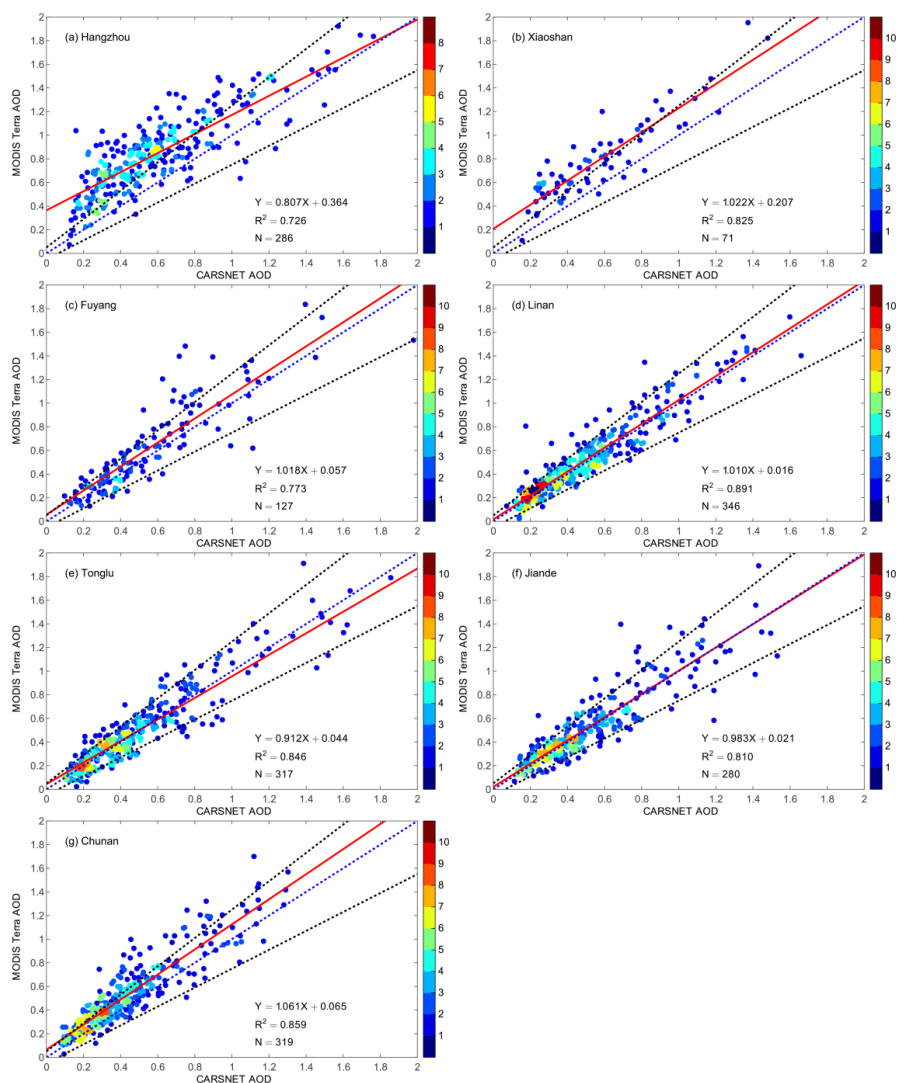
251

252 Fig. 3. (a) Annual variation in the EAE at 440–870 nm. Variation in the EAE at 440–870 nm



253 over (b) Hangzhou, (c) Xiaoshan, (d) Fuyang, (e) LinAn, (f) Tonglu, (g) Jiande and (h) ChunAn.
254 The boxes represent the 25th to 75th percentile distribution, while the dots and solid lines
255 within each box represent the mean and median, respectively.

256 Validation of the MODIS C6 retrieval AOD values was carried out by comparison with
257 ground-based observations (Figure 4). The systematic performance of the MODIS C6 retrieval
258 AOD values was generally stable in the YRD region, with most of the plots scattered around
259 the 1:1 regression line. The correlation coefficients (R^2) between the Terra-MODIS and sun
260 photometer AOD (550 nm) values were about 0.73, 0.83, 0.77, 0.89, 0.85, 0.81 and 0.86 at
261 Hangzhou, Xiaoshan, Fuyang, LinAn, Tonglu, Jiande and ChunAn, respectively. The linear
262 regression fitting performed better at the suburban sites of LinAn and Jiande. The fitting curve
263 was almost consistent with the 1:1 reference line, which suggests that the aerosol properties
264 were well defined for the MODIS C6 products. A large part of the MODIS retrieval AOD value
265 was outside the expected error envelope of $\pm (0.05 + 20\%T_{\text{CARSNET}})$, especially for AOD values
266 < 0.80 in Hangzhou and Xiaoshan. This indicates that the MODIS retrieval algorithm could still
267 be improved, especially in urban areas. The MODIS retrieval AOD performed better at the
268 other five sites (Fuyang, LinAn, Tonglu, Jiande and ChunAn) in the YRD; most of the retrieved
269 AOD values for these sites fell within the expected error envelope. The MODIS retrievals were
270 overestimated at Hangzhou, Xiaoshan and ChunAn. This could be because the MODIS SSA
271 was underestimated at and near to urban sites (Tao et al., 2015). The small deviation at the
272 suburban sites suggested that the MODIS C6 retrieval method was suitable for capturing the
273 optical properties of aerosols in suburban areas of the YRD.



274

275 Fig. 4. Comparison of C6 MODIS AOD at 550 nm with the CARSNET AOD in (a)
276 Hangzhou, (b) Xiaoshan, (c) Fuyang, (d) LinAn, (e) Tonglu, (f) Jiande and (g) ChunAn. The red
277 solid line represents the linear regression. The two black dotted lines represent the expected
278 errors in the MODIS retrievals.

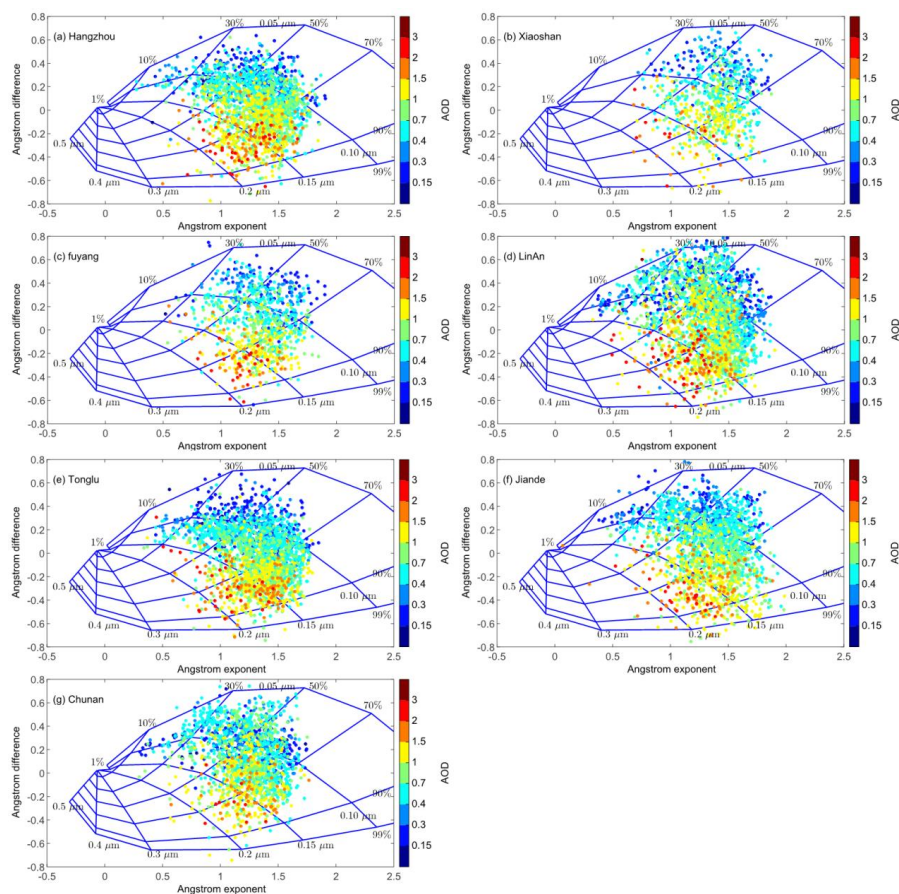
279 The relationship between the EAE and the spectral difference in the EAE
280 ($\delta\text{EAE} = \text{EAE}_{440-675\text{nm}} - \text{EAE}_{675-870\text{nm}}$) was analyzed to investigate the contribution of fine



281 particles (R_i) and their fraction (η) to the total extinction (EAOD) at 440 nm (Gobbi et al., 2007).
282 In this framework, values of $AOD > 0.15$ are represented by different colors to avoid errors in
283 the δEAE . The lines indicate contribution of the fixed radius (R_i) and fraction (η) of the
284 fine-mode particles to the total extinction. Gobbi et al. (2007) used the difference in the EAE
285 and AOD data to determine the growth of fine-mode particles or contamination by
286 coarse-mode particles at eight AERONET stations: Beijing (China), Rome (Italy), Kanpur
287 (India), Ispra (Italy), Mexico City (Mexico), NASA Goddard Space Flight Center (GSFC, USA),
288 Mongu (Zambia) and Alta Floresta (Brazil).

289 Fig. 5 shows that the high EAOD values (> 1.00) cluster in the plots for all seven urban,
290 suburban and rural sites, which is attributed to fine-mode particles with $\delta EAE < 0$ and $\eta \sim 50$ –
291 90%. This variation in the fine-mode particles is similar to the results from Beijing and Kanpur
292 ($\eta \sim 70$ –90%). However, there were very few coarse-mode particles ($\delta EAE \sim 0$, $\eta \sim 0$ –10%) in
293 this study, suggesting that the dominance of dust is not significant in eastern China. These
294 results showed a different pattern from that of other regions in north/northeast China (Wang et
295 al., 2010; Zhu et al., 2014). For $\delta EAE \sim 0$ and $10\% < \eta < 30\%$, high extinction was associated
296 with a mixture dominated by fine-mode particles and less persistent coarse-mode particles.
297 Clustering concentrated in the region $\alpha \sim 1.5$, $\delta \alpha \sim -0.5$ with high AOD values at all sites, which
298 may be linked to an increase in size of the fine-mode particles by coagulation as they aged
299 and hygroscopic events, as seen at other locations (e.g. Ispra, Italy; Mexico City, Mexico;
300 GSFC, USA).

301



302

303 Fig. 5. Angström exponent difference as a function of $\alpha_{440-870 \text{ nm}}$ and the $\text{AOD}_{440 \text{ nm}}$ over (a)
304 Hangzhou, (b) Xiaoshan, (c) Fuyang, (d) LinAn, (e) Tonglu, (f) Jiande and (g) ChunAn.

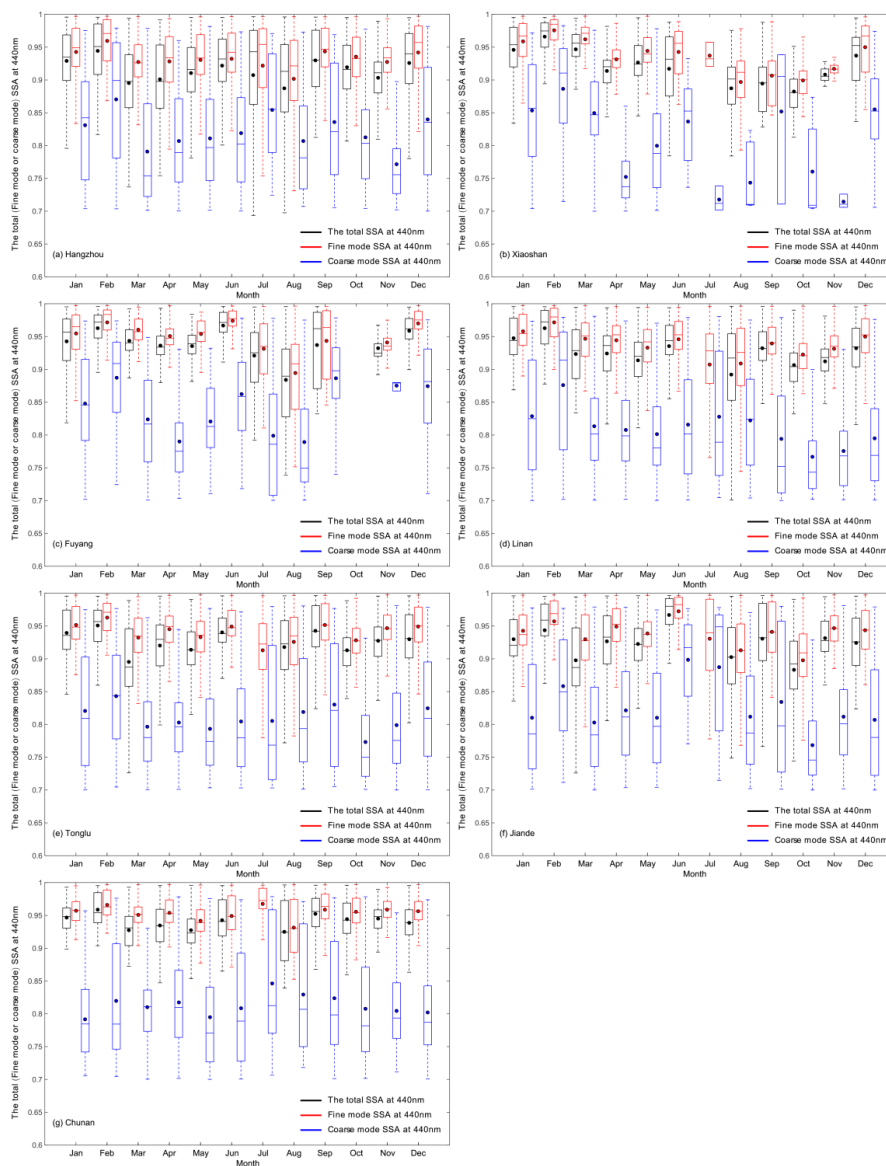
305 3.2 Single-scattering albedo and aerosol complex refractive index

306 The distribution of the total, fine- and coarse-mode SSAs at seven sites in the YRD are
307 shown in Fig. 6. The total SSA varied from 0.91 to 0.94, which is similar to the range seen in
308 other regions of China, such as Wuhan (0.92), Beijing (0.89) and Xinglong (0.92) (Wang et al.,
309 2015; Xin et al., 2014; Zhu et al., 2014). This indicated that scattering aerosol particles in
310 eastern China resulting from high levels of industrial and anthropogenic activity were dominant.
311 The characteristics of the SSA at these seven sites gradually increased from the east coast
312 (0.91 ± 0.06 at Hangzhou) inland toward the west (0.94 ± 0.03 at ChunAn). These results



313 indicate the emissions caused by human activity affect the absorption of aerosols in urban
314 areas. The SSA was higher at LinAn and ChunAn than at the other sites, which may reflect the
315 presence of a larger number of scattering aerosols (e.g. particles from urban/industrial
316 activities) over the regional background/rural sites than over urban or suburban sites. The SSA
317 over urban and suburban sites showed the largest monthly variation. The monthly average
318 values of SSA_t were high in February (-0.94 ± 0.05) and June (-0.92 ± 0.06), but low in March
319 (-0.90 ± 0.06) and August (-0.89 ± 0.09) in Hangzhou. However, the monthly SSA values at the
320 rural site of ChunAn only varied from 0.92 to 0.95. We concluded that the type of aerosol at
321 urban/suburban sites was more complex than at rural sites.

322 The range of variation in the SSA of fine particles (SSA_t) was 0.93–0.95, whereas the SSA
323 for coarse-mode particles (SSA_c) was 0.81–0.84 at the seven sites (Fig. 6). The fine- and
324 coarse-mode particles displayed significant scattering and absorption abilities in the urban,
325 suburban and rural areas of the YRD region. Fig. 6 shows a significant decrease in the
326 fine-mode SSA in July/August and in the coarse-mode SSA in March/April. At Hangzhou, the
327 lower fine-mode SSA values in July/August (-0.92 ± 0.08 / -0.90 ± 0.08) were probably a result of
328 aerosols from biomass burning and the lower coarse-mode SSA values in March/April
329 (-0.79 ± 0.08 / -0.81 ± 0.07) may reflect the existence of light-absorbing dust aerosols (Yang et al.,
330 2009). The SSA depends on the wavelength and dust particles absorb strongly at short
331 wavelengths, resulting in a lower SSA at 440 nm (Eck et al., 2010). The absorption/scattering
332 properties of fine- and coarse-mode particles determine the total SSA in the YRD. These
333 differences in the SSA were mostly dependent on the type of aerosol and the ratio of absorbing
334 and non-absorbing components in the aerosols.



335

336 Fig. 6. Variation in the total, fine- and coarse-mode $SSA_{440\text{ nm}}$ over (a) Hangzhou, (b) Xiaoshan,
337 (c) Fuyang, (d) LinAn, (e) Tonglu, (f) Jiande and (g) ChunAn. The boxes represent the 25th to
338 75th percentile distribution, while the dots and solid lines within each box represent the mean
339 and median, respectively.

340 The real and imaginary parts of the refractive index represent the scattering and



341 absorption capacity of particles, respectively. The refractive index is determined by the
342 hygroscopic conditions and the chemical composition of the aerosols (Dubovik and King,
343 2000). There was no significant difference between the real parts of the refractive index among
344 the seven urban, suburban and rural sites in this study (range 1.41–1.43). The real parts of the
345 refractive index in this study were smaller than the real parts of ammonium sulfate and
346 ammonium nitrate (1.55), which may be due to the hygroscopic conditions or the mixture of
347 dust particles. The real part of the refractive index was highest in March ($\sim 1.46 \pm 0.06$) and
348 November ($\sim 1.45 \pm 0.06$) and lowest in July ($\sim 1.42 \pm 0.06$) and August ($\sim 1.41 \pm 0.07$) at the urban
349 sites. A higher level of dust aerosols with weak scattering in spring and autumn could
350 contribute to a higher value of the real part of the refractive index; this was reduced or
351 eliminated by rainfall during the summer months.

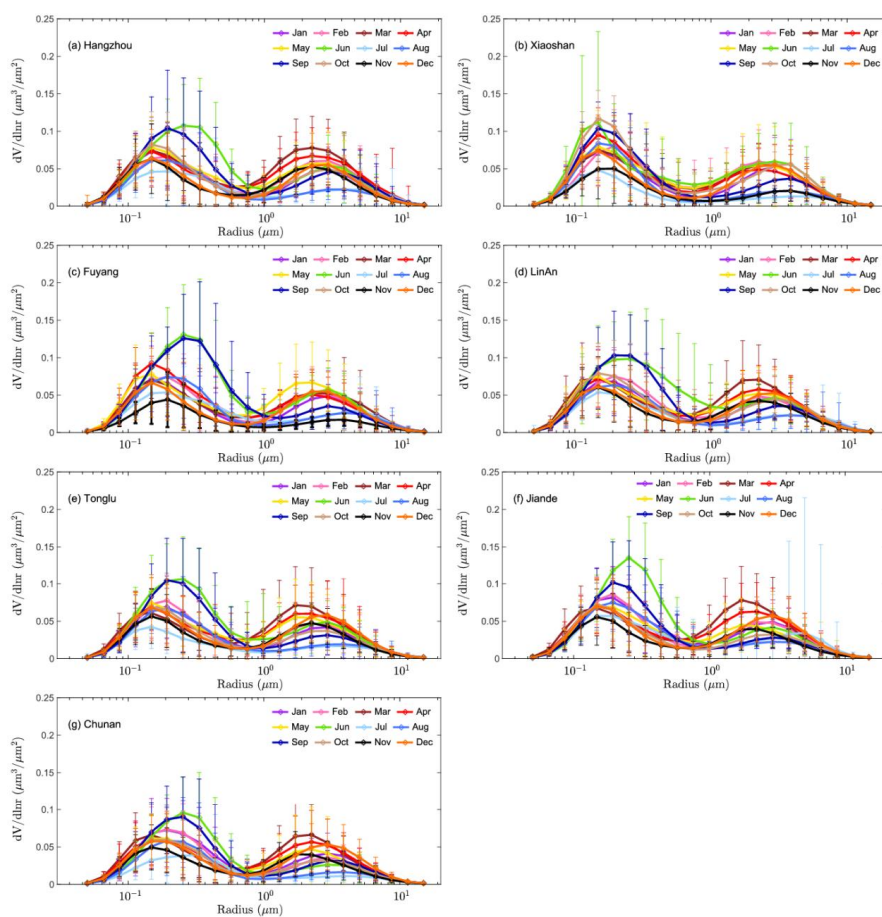
352 The imaginary part of the refractive index was higher at the urban site of Hangzhou
353 ($\sim 0.0112 \pm 0.0104$) as a result of the high loading of absorption aerosols in this region and was
354 consistent with the lower SSA. High imaginary parts of the refractive index occurred in August
355 at all urban, suburban and rural sites in the YRD, which may be due to the higher emission of
356 absorptive particles by the post-harvest burning of crop residues. The burning of crop residues
357 may cause a large deterioration in the regional air quality in the YRD region.

358 3.3 Radius and aerosol volume size distributions

359 Fig. 7 shows the monthly aerosol size distribution ($dV/d\ln r$) in the YRD for all sites. The
360 volumes of fine-mode aerosols were obviously higher than those of coarse-mode aerosols
361 over all sites. The fine-mode radii were ~ 0.2 – $0.3 \mu\text{m}$ in the YRD with a volume of 0.10 – 0.12
362 μm^3 and the coarse-mode radii were $\sim 2.0 \mu\text{m}$ with a volume close to $0.07 \mu\text{m}^3$. The amount of
363 fine-mode aerosols was higher in June and September than in other months at almost sites,
364 except for Xiaoshan. This could be caused by aerosol humidification (Eck et al., 2012; Li et al.,
365 2010, 2014; Huang et al., 2016). This phenomenon is also found over Beijing and Shenyang in
366 north/northeast China, suggesting that hygroscopic growth occurs over many regions of China
367 (Li et al., 2011; Che et al., 2015c).



368 The coarse-mode radius in spring at all sites was smaller than in other cities in north and
369 northeast China affected by frequent dust transport events in spring (Kong et al., 2011; Zhao et
370 al., 2015). The coarse-mode particles showed a larger effective radius at all seven urban,
371 suburban and rural sites in the summer, which may due to the adhesion of new particles onto
372 larger particles (such as fly ash).



373

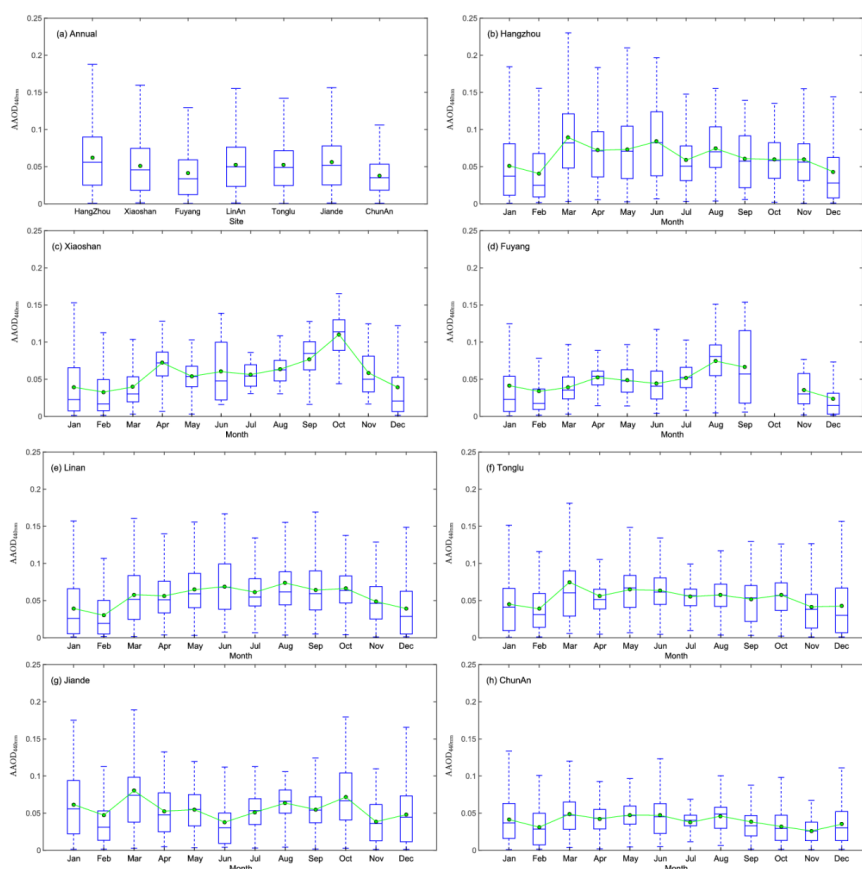
374 Fig. 7. Variation in the annual volume size distribution over (a) Hangzhou, (b) Xiaoshan, (c)
375 Fuyang, (d) LinAn, (e) Tonglu, (f) Jiande and (g) ChunAn.

376 3.4 Absorption aerosol optical depth and absorption Angström exponent

377 The annual AAODs at Hangzhou, Xiaoshan, Fuyang, LinAn, Tonglu, Jiande and ChunAn



378 were about 0.06 ± 0.05 , 0.05 ± 0.04 , 0.04 ± 0.04 , 0.05 ± 0.04 , 0.05 ± 0.04 , 0.06 ± 0.04 and 0.04 ± 0.03 ,
379 respectively (Fig. 8). The higher annual values of the AAOD in Hangzhou and Jiande indicate
380 that there are more absorbing aerosol particles at these sites. The similar AAOD level at the
381 seven sites suggests that absorbing aerosols are distributed homogeneously in the YRD
382 region. The monthly AAOD at the urban site of Hangzhou was 0.09 ± 0.06 in March as a result
383 of the presence of absorbing dust particles. The AAOD of about 0.07 ± 0.04 in August is related
384 to the burning of crop residues. The AAODs in the winter season at all the sites in the YRD
385 region were < 0.05 , which suggests that absorbing aerosol emissions did not frequently occur
386 at these sites, unlike in the northern regions of China.



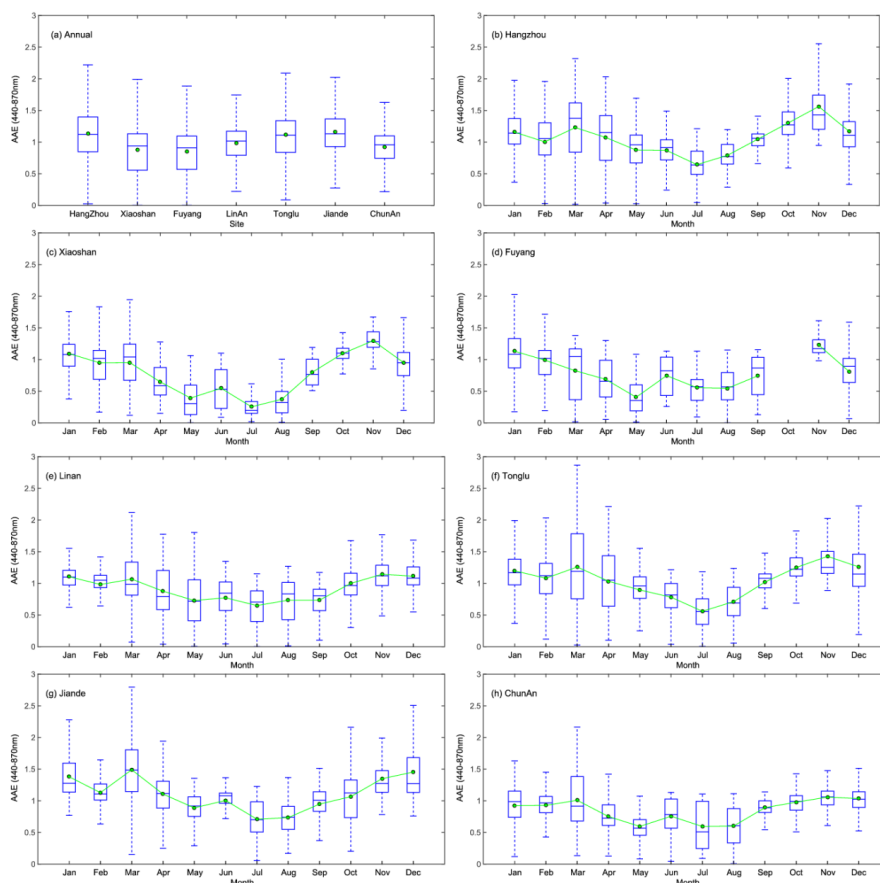
387

388 Fig. 8. (a) Annual variation in the absorption aerosol optical depth at 440 nm ($AAOD_{440\text{ nm}}$) over



389 (b) Hangzhou, (c) Xiaoshan, (d) Fuyang, (e) LinAn, (f) Tonglu, (g) Jiande and (h) ChunAn. The
390 boxes represent the 25th to 75th percentile distribution, while the dots and solid lines within
391 each box represent the mean and median, respectively.

392 The annual mean values for the AAE at Hangzhou, Xiaoshan, Fuyang, LinAn, Tonglu,
393 Jiande and ChunAn were about 1.13 ± 0.46 , 0.88 ± 0.42 , 0.85 ± 0.43 , 0.98 ± 0.35 , 1.11 ± 0.49 ,
394 1.16 ± 0.44 and 0.93 ± 0.31 , respectively (Fig. 9). The mean values of the AAE at Xiaoshan and
395 Fuyang were < 1.00 , suggesting the presence of absorbing or non-absorbing materials coating
396 black carbon at these suburban and rural sites (Bergstrom et al., 2007; Lack and Cappa et al.,
397 2010; Gyawali et al., 2009). The AAE values were close to 1.00 at LinAn and ChunAn,
398 indicating that the absorptive aerosols were dominated by particles of black carbon (Zhang et
399 al., 2012; Li et al., 2016). By contrast, the AAE values at Hangzhou, Tonglu and Jiande
400 were > 1.00 , indicating the presence of absorptive aerosols from the burning of biomass. This
401 difference in the AAE distribution indicates the absorbing aerosols have different
402 characteristics resulting from the different emission sources at urban, suburban and rural sites
403 in the YRD. The AAE was < 1.00 in June – August at all urban, suburban and rural sites of the
404 YRD, which suggested the presence aerosols coated with absorbing or non-absorbing
405 material in summer season. This process is favored by high temperatures and high humidity
406 under conditions of strong solar radiation (Shen et al., 2015, Zhang et al., 2015). The particles
407 coagulate and grow rapidly in the presence of sufficient water vapor (Li et al., 2016). The AAE
408 became increasingly close to, or larger than, 1.00 at all seven sites from September, which is
409 consistent with decreasing amounts of precipitation. This increase in the AAE was related to
410 the emission of black carbon from biomass burning (Soni et al., 2010; Russell et al., 2010).



411

412 Fig. 9. (a) Annual variation in the absorption Angström exponent at 440 nm ($AAE_{440\text{ nm}}$) over (b)
413 Hangzhou, (c) Xiaoshan, (d) Fuyang, (e) LinAn, (f) Tonglu, (g) Jiande and (h) ChunAn. The
414 boxes represent the 25th to 75th percentile distribution, while the dots and solid lines within
415 each box represent the mean and median, respectively.

416 The AAE can be used to indicate the major types (urban/industrial, biomass burning,
417 dust/mixed dust) or optical mixtures of absorbing aerosol particles (Schnaiter et al., 2006;
418 Russell et al., 2010; Giles et al., 2011; 2012; Mishra and Shibata, 2012). Giles et al., (2011)
419 examined AAE/EAE data from Kanpur to classify the categories of absorbing aerosols. The
420 “mostly dust” category has been defined as having an EAE value ≤ 0.50 and sphericity fraction
421 < 0.20 with an AAE value > 2.00 . The “mostly black carbon” category has been defined as



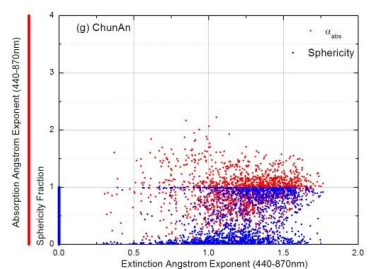
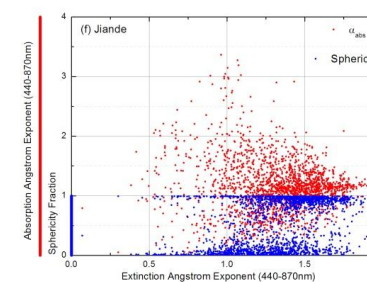
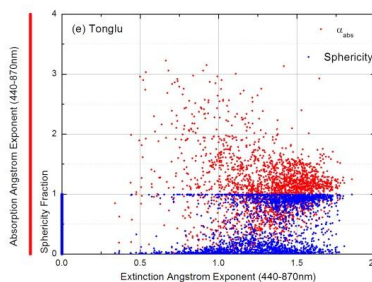
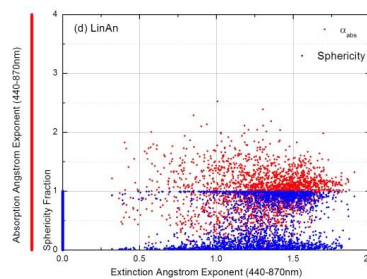
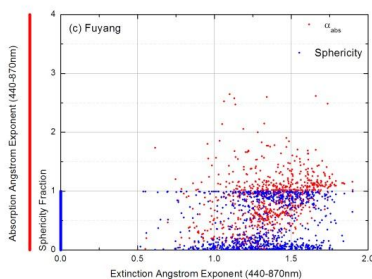
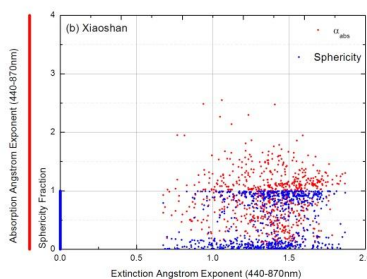
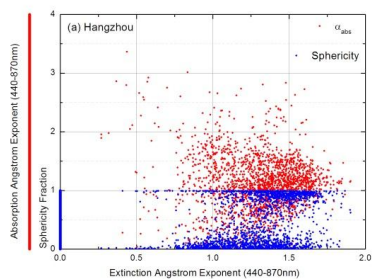
422 having an EAE value >0.80 and a sphericity fraction ≥ 0.20 with $1.00 < \text{AAE} \leq 2.00$. Values of
423 EAE >0.80 and AAE >2.00 indicate a concentration of organic carbon (Arola et al., 2011). The
424 “mixed black carbon and dust” category was centered at EAE ~ 0.50 with AAE ~ 1.50 and used
425 to represent an optical mixture with black carbon and mineral dust particles as the dominant
426 absorbers.

427 We used the instantaneous AAE and EAE values to classify the dominant absorbing
428 aerosol types in urban, suburban and rural areas of the YRD (Fig. 10; Table 2). Table 2 shows
429 that the “mostly dust” category was very low at both suburban and rural sites ($<0.01\%$) and just
430 $\sim 0.24\%$ at the urban site of Hangzhou. This indicates that dust does not dominate the
431 absorbing aerosol particles in the YRD region of eastern China, which is completely different
432 from other regions of north/northeast China. The “mostly black carbon” category dominates the
433 absorbing aerosols in the urban, suburban and rural areas in the YRD region. The percentage
434 “mostly black carbon” varied from ~ 20 to 40% depending on each site, indicating the mixing of
435 black carbon as well as brown and soot carbon species from biomass burning and
436 urban/industrial activities. Because of the long-distance transportation and local fugitive dust
437 effect, the “mixed black carbon and dust” category contributed $\sim 5\%$ of the absorbing aerosol
438 particles in the YRD region. There were also $\sim 1 - 4\%$ of the “organic carbon” category
439 identified as absorbing aerosol particles in this region. Particles with EAE values of ~ 0.40 and
440 ~ 1.25 could be regarded as “mixed large particles” greater than microns in size and submicron
441 “mixed small particles”, respectively (Giles et al. 2012). The frequency of “mixed large particles”
442 was $<0.5\%$ at the urban, suburban and rural sites (Table 2). By contrast, the frequency of
443 “mixed small particles” was $\sim 18 - 36\%$.

444 The EAE (α_{ext}) and AAE (α_{abs}) values at all the urban, suburban and rural sites were
445 distributed mainly around 1.25 and $1.00 - 1.50$ (Fig. 10), respectively. In contrast with the
446 results of Giles et al. (2011), the sphericity fraction did not show an obvious transition from
447 non-spherical to spherical particles from the urban, suburban and rural sites in YRD. The
448 sphericity fraction showed a dispersed distribution of spherical particles, indicating a mixture of
449 fine-mode particles derived from anthropogenic sources and coarse-mode particles, such as



450 dust events transported from north/northwest China or local fugitive dust emissions.





455 Fig. 10. The AAE and the sphericity fraction as a function of the EAE at 440–870 nm over (a)
456 Hangzhou, (b) Xiaoshan, (c) Fuyang, (d), LinAn, (e) Tonglu, (f) Jiande and (g) ChunAn.

457 Table 2. Types of aerosol at the seven sites in the Yangtze River Delta.

	Mostly dust (%)	Mixed black carbon and dust (%)	Mostly black carbon (%)	Organic carbon (%)	Mixed large particles (%)	Mixed small particles (%)
Hangzhou	0.24	6.14	34.68	2.58	0.19	36.34
Xiaoshan	<0.01	2.93	27.00	0.80	<0.01	23.40
Fuyang	<0.01	1.21	19.51	1.10	<0.01	18.63
LinAn	<0.01	6.18	28.91	0.50	0.37	28.04
Tonglu	<0.01	4.92	34.26	3.55	0.18	33.33
Jiande	<0.01	6.71	40.04	3.23	0.26	35.28
ChunAn	<0.01	7.16	24.15	0.23	0.12	26.75

458

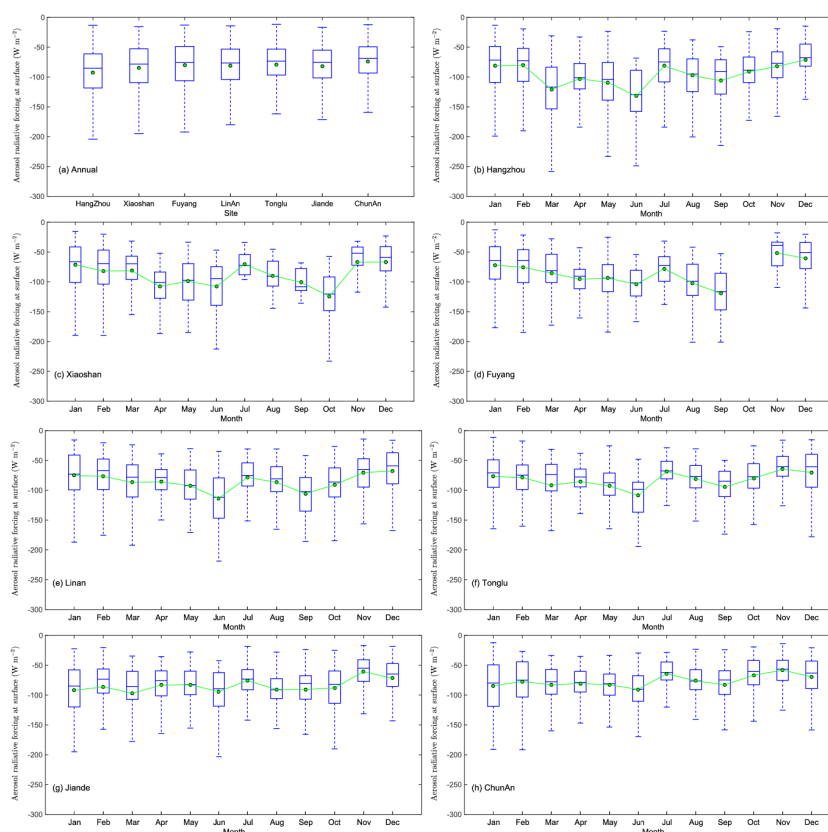
459 3.5 Aerosol radiative forcing at the Earth's surface and top of the atmosphere

460 Figures 11 and 12 show the variations in ARF at the surface (ARF-BOA) and at the top of
461 the atmosphere (ARF-TOA) at the urban, suburban and rural sites in the YRD region.

462 The annual ARF-BOA values for Hangzhou, Xiaoshan, Fuyang, LinAn, Tonglu, Jiande and
463 ChunAn were about -93 ± 44 , -84 ± 40 , -80 ± 40 , -81 ± 39 , -79 ± 39 , -82 ± 40 and -74 ± 34 W/m^2 ,
464 respectively. The higher ARF-BOA values in Hangzhou indicate that there was high aerosol
465 loading at this site, which scattered and absorbed more radiation and caused a significant
466 cooling effect at the surface. The monthly value of the ARF-BOA in Hangzhou was higher in
467 June (about -132 ± 48 W/m^2) and September (about -106 ± 48 W/m^2), which is consistent with
468 the timing of burning biomass from crop residues. Ding et al. (2016) found that black carbon
469 emitted from biomass burning can modify the meteorology of the planetary boundary layer and
470 substantially decrease the surface heat flux. Hygroscopic growth at the same time enhances



471 the aerosol optical extinction (Yan et al., 2009; Zhang et al., 2015); this was also an important
472 factor in the large ARF-BOA values in June and September at the urban, suburban and rural
473 sites in the YRD.



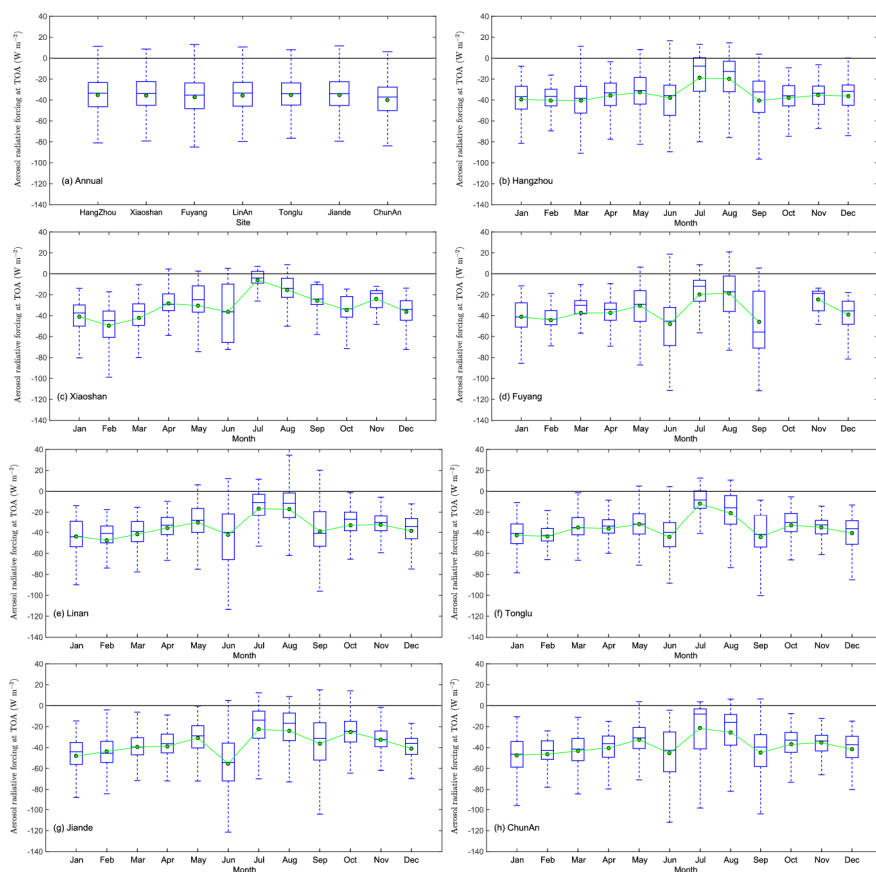
474

475 Fig. 11. (a) Annual variation of the ARF at the surface over (b) Hangzhou, (c) Xiaoshan, (d)
476 Fuyang, (e) LinAn, (f) Tonglu, (g) Jiande and (h) ChunAn. The boxes represent the 25th to 75th
477 percentile distribution, while the dots and solid lines within each box represent the mean and
478 median, respectively.

479 The ARF-TOA values were less than -40 W/m^2 at the urban, suburban and rural sites in
480 the YRD. The AFR-TOA values were negative all year, which suggests that the aerosols
481 caused a cooling effect at the TOA as well as at surface in the YRD. This is different from the



482 north/northeast regions of China, where the instantaneous AFR-TOA value can be positive in
483 the winter season as a result of the large surface area reflecting short wavelength radiation
484 and heating caused by absorbing aerosols (Che et al., 2014). The surface albedo in the YRD
485 region is lower than in north/northeast China as a result of better vegetation. At the same time,
486 there is also a low level of absorbing aerosol emissions in winter. This caused obvious
487 negative AFR at the TOA at the urban, suburban and rural sites in the YRD.



488
489 Fig. 12. (a) Annual variation in the aerosol radiative forcing at the top of the atmosphere (TOA)
490 in (b) Hangzhou, (c) Xiaoshan, (d) Fuyang, (e) LinAn, (f) Tonglu, (g) Jiande and (h) ChunAn.
491 The boxes represent the 25th to 75th percentile distribution, while the dots and solid lines
492 within each box represent the mean and median, respectively.



493 **4. Summary and discussion**

494 The aerosol optical properties, including the AOD, EAE, SSA, complex refractive index,
495 volume size distribution, and the absorption properties of the AAOD and AAE were retrieved
496 from satellite data over the YRD in eastern China for the period 2011–2015.

497 Aerosol loading was at a high level over both urban and suburban sites and even over the
498 rural sites in the YRD, which suggests that pollution from aerosols is not just local, but has
499 occurred at a regional scale over eastern China in recent years. The AOD showed a
500 decreasing trend from the east coast inland to the west as a result of contributions from
501 anthropogenic activity. Hygroscopic growth and the burning of biomass from crop residues in
502 the summer season could cause this obvious increase in the AOD. The ratio of $AOD_{0.47}/AOD_{0.66}$
503 was consistently >0.90 , indicating that fine-mode particles made a major contribution to the
504 total AOD in the YRD. The relationship between the EAE and the spectral difference in the
505 EAE suggested that the dominance of dust is not important in eastern China. The MODIS C6
506 AOD retrievals performed better in suburban than in urban and rural areas, but were
507 systematically overestimated in rural and urban areas and their immediate surroundings. A
508 large part of the MODIS retrieval AOD was outside the expected error, especially at AOD
509 values <0.80 in urban areas and their immediate surroundings.

510 The range of variation of the total, fine- and coarse-mode SSA values was 0.91–0.94,
511 0.93–0.95 and 0.81–0.84, respectively, in the YRD region, suggesting the presence of mainly
512 scattering aerosol particles in eastern China as a result of high industrial and anthropogenic
513 activity. The fine- and coarse-mode particles showed significant scattering and absorption in
514 the urban, suburban and rural areas of the YRD region. The imaginary part of the refractive
515 index was larger at urban sites as a result of the high loading of absorption aerosols. The large
516 imaginary parts occurring in August may be due to the higher emission of absorptive particles
517 from the post-harvest burning of biomass.

518 The similar AAOD levels at the seven sites indicated that absorbing aerosols were
519 homogeneously distributed in the YRD region. The low AAODs in the winter season suggest



520 fewer absorbing aerosol emissions at the urban, suburban and rural sites. The difference in
521 the distribution of the AAE suggests that the absorbing aerosols have different characteristics
522 depending on the emission source. Hygroscopic growth not only contributed to the high
523 aerosol extinction values, but also increased the size of the fine-mode particles in the summer
524 in the YRD region. The “mostly black carbon” category was the dominant contributor of
525 absorbing aerosols at the urban, suburban and rural sites in the YRD region. The submicron
526 “mixed small particle” category had a significant effect on the aerosol optical properties over
527 the YRD region. The sphericity fraction showed a dispersed distribution of spherical particles,
528 indicating a mixture of both fine- and coarse-mode particles from anthropogenic and natural
529 sources.

530 The large ARF-BOA indicated a high aerosol loading that scattered and absorbed more
531 radiation. It also showed that the cooling effect of the aerosols at the surface was stronger in
532 the YRD region. Both the burning of biomass from crop residues and the hygroscopic growth
533 of particles could make important contributions to the ARF-BOA in summer over the YRD
534 region. The AFR-TOA values were negative all year, suggesting that the aerosols had a
535 cooling effect at the TOA.

536 The column aerosol optical properties over urban, suburban and rural areas of YRD
537 region of China were investigated and the results will increase our understanding of the
538 characteristics and sources of aerosol emissions over eastern China. Future research should
539 consider the vertical distribution of aerosols by Lidar, the validation of the aerosol optical
540 results of other satellite products such as VIIRS and GOCI, and a comprehensive analysis of
541 the physical and chemical properties of aerosols and meteorological factors.

542 **Acknowledgments**

543 This work was supported by grant from National Key R & D Program Pilot Projects of
544 China (2016YFA0601901), National Natural Science Foundation of China (41590874
545 &41375153), Natural Science Foundation of Zhejiang Province (LY16010006), the CAMS
546 Basis Research Project (2016Z001 & 2014R17), the Climate Change Special Fund of CMA



547 (CCSF201504), CAMS Basic Research Project (2014R17), the Special Project of Doctoral
548 Research supported by Liaoning Provincial Meteorological Bureau (D201501), Hangzhou
549 Science and Technology Innovative project (20150533B17) and the European Union Seventh
550 Framework Programme (FP7/2007-2013) under grant agreement no. 262254.

551 **Reference**

552 Ackerman, P., and Toon, O.B.: Absorption of visible radiation in atmosphere containing
553 mixtures of absorbing and nonabsorbing particles, *Appl. Opt.*, 20, 3661-3668, 1981.

554 Albrecht, B.: Aerosols, cloud microphysics, and fractional cloudiness, *Science*, 245,
555 1227-1230, 1989.

556 Arola, A., Schuster, G., Myhre, G., Kazadzis, S., Dey, S., and Tripathi, S. N.: Inferring
557 absorbing organic carbon content from AERONET data, *Atmos. Chem. Phys.*, 11, 215–
558 225, doi:10.5194/acp-11-215-2011, 2011.

559 Bergstrom, R.W., Pilewskie, P., Russell, P.B., Redemann, J., Bond, T.C., Quinn, P.K., and
560 Sierau, B.: Spectral absorption properties of atmospheric aerosols, *Atmos. Chem. Phys.*,
561 7, 5937–5943, doi: 10.5194/ acp-7-5937-2007, 2007.

562 Charlson, R.J., Schwartz, S.E., Hales, J.M., Cess, D., Coakley, J.A., and Hansen, J.E.:
563 Climate forcing by anthropogenic aerosols, *Science*, 255, 423–430, 1992.

564 Che, H.Z., Xia, X.A., Zhu, J., Wang, H., Wang, Y.Q., Sun, J.Y., Zhang, X.C., Zhang, X.Y., and
565 Shi, G.Y.: Aerosol optical properties under the condition of heavy haze over an urban site
566 of Beijing, China, *Environ. Sci. Pollut. Res.*, 22, 1043–1053, 2015a.

567 Che, H. Z., Zhang, X. Y., Alfraro, S., Chatenet, B., Gomes, L., and Zhao, J. Q.: Aerosol optical
568 properties and its radiative forcing over Yulin, China in 2001 and 2002, *Adv. Atmos. Sci.*,
569 26, 564–576, doi:10.1007/s00376-009-0564-4, 2009b.

570 Che, H., Zhang, X., Chen, H., Damiri, B., Goloub, P., Li, Z., Zhang, X., Wei, Y., Zhou, H., Dong,
571 F., Li, D., and Zhou, T.: Instrument calibration and aerosol optical depth (AOD) validation
572 of the China Aerosol Remote Sensing Network (CARSNET), *J. Geophys. Res.*, 114, doi:
573 org/10.1029/2008JD011030, 2009a.

574 Che, H., Yang, Z., Zhang, X., Zhu, C., Ma, Q., Zhou, H., and Wang, P.: Study on the aerosol
575 optical properties and their relationship with aerosol chemical compositions over three



- 576 regional background stations in China, *Atmos. Environ.*, 43, 1093–1099,
577 doi:10.1016/j.atmosenv.2008.11.010, 2009c.
- 578 Che, H., Wang, Y., Sun, J., and Zhang, X.: Assessment of In-situ Langley Calibration of
579 CE-318 Sunphotometer Mt. Waliguan Observatory, China, *SOLA*, 7, 089-092, doi:
580 10.2151/sola.2011-023, 2011
- 581 Che, H., Wang, Y., and Sun, J.: Aerosol optical properties at Mt.Waliguan observatory, China,
582 *Atmos. Environ.*, 45, 6004–6009, 2011.
- 583 Che, H.Z., Zhang, X.Y., Xia, X.A., Goloub, P., Holben, B., Zhao, H., Wang, Y., Zhang, X.C.,
584 Wang, H., and Blarel, L. et al.: Ground-based aerosol climatology of China: Aerosol
585 optical depths from the China Aerosol Remote Sensing Network (CARSNET) 2002–2013,
586 *Atmos. Chem. Phys.*, 15, 7619–7652, 2015b.
- 587 Che, H.Z., Zhao, H.J., Xia, X.A., Wu, Y.F., Zhu, J., Ma, Y.J., Wang, Y.F., Wang, H., Wang, Y.Q.,
588 Zhang, X.Y., and Shi, G.Y.: Fine Mode Aerosol Optical Properties Related to Cloud and
589 Fog Processing over a Cluster of Cities in Northeast China, *Aerosol. Air. Quality*
590 *Research.*, 15, 2065–2081, 2015c.
- 591 Che, H.Z., Xia, X.A., Zhu, J., Wang, H., Wang, Y.Q., Sun, J.Y., Zhang, X.C., Zhang, X.Y., and
592 Shi, G.Y.: Aerosol optical properties under the condition of heavy haze over an urban site
593 of Beijing, China, *Environ. Sci. Pollut. Res.*, <http://dx.doi.org/10.1007/s11356-014-3415-5>,
594 2014.
- 595 Cheng, T.T., Xu, C., Duan, J.Y., Wang, Y.F., Leng, C.P., Tao, J., Che, H.Z., He, Q.S., Wu, Y.F.,
596 Zhang, R.J., Li, X., Chen, J.M., Kong, L.D., and Yu, X.N.: Seasonal variation and
597 difference of aerosol optical properties in columnar and surface atmospheres over
598 Shanghai, *Atmos. Environ.*, 123, 315-326, 2015.
- 599 Chu, D.A., Kaufman, Y.J., Ichoku, C.: Validation of MODIS aerosol optical depth retrieval over
600 land, *Geophysics Research Letters*, 29 (12), 8007, 2002.
- 601 Ding, A. J., Fu, C. B., Yang, X. Q., Sun, J. N., Zheng, L. F., Xie, Y. N., Herrmann, E., Nie, W.,
602 Petäjä, T., Kerminen, V.-M., and Kulmala, M.: Ozone and fine particle in the western
603 Yangtze River Delta: an overview of 1 yr data at the SORPES station, *Atmos. Chem.*
604 *Phys.*, 13, 5813–5830, doi:10.5194/acp-13-5813-2013, 2013a.
- 605 Ding, A. J., Fu, C. B., Yang, X. Q., Sun, J. N., Petäjä, T., Kerminen, V.-M., Wang, T., Xie, Y.,



- 606 Herrmann, E., Zheng, L. F., Nie, W., Liu, Q., Wei, X. L., and Kulmala, M.: Intense
607 atmospheric pollution modifies weather: a case of mixed biomass burning with fossil fuel
608 combustion pollution in eastern China, *Atmos. Chem. Phys.*, 13, 10545-10554,
609 doi:10.5194/acp-13-10545-2013, 2013b.
- 610 Ding, A. J., Huang, X., Nie, W., Sun, J. N., Kerminen, V.M., Petäjä, T., Su, H., Cheng, Y. F.,
611 Yang, X.Q., and Wang, M.H. et al.: Enhanced haze pollution by black carbon in megacities
612 in China, *Geophys. Res. Lett.*, 43, 2873–2879, doi: 10.1002/2016GL067745, 2016.
- 613 Duan, J., Mao, J.: Study on the distribution and variation trends of atmospheric aerosol optical
614 depth over the Yangtze River Delta, *Acta Scientiae Circumstantiae*, 27 (4), 537-543, 2007.
- 615 Dubovik, O., Holben, B.N., Eck, T.F., Smirnov, A., Kaufman, Y.J., King, M.D., Tanre, D.,
616 Slutsker, I.: Variability of absorption and optical properties of key aerosol types observed
617 in worldwide locations, *J. Atmos. Sci.*, 59, 590–608, 2002.
- 618 Dubovik, O., King, M.D.: A flexible inversion algorithm for retrieval of aerosol optical properties
619 from Sun and sky radiance measurements, *J. Geophys. Res.*, 105 (D16), 20673, 2000.
- 620 Dubovik, O., Sinyuk, A., Lapyonok, T., Holben, B.N., Mishchenko, M., Yang, P., Eck, T.F.,
621 Volten, H., Munoz, O., Veihelmann, B., van der Zande, W.J., Leon, J.F., Sorokin, M., and
622 Slutsker, I.: Application of spheroid models to account for aerosol particle nonsphericity in
623 remote sensing of desert dust, *J. Geophys. Res.-Atmos.*, 111 (D11), 2006.
- 624 Dubuisson, P., Buriez, J.C., and Fouquart, Y.: High spectral resolution solar radiative transfer
625 in absorbing and scattering media, application to the satellite simulations, *J. Quant.
626 Spectrosc. Radiat. Transf.*, 55, 103–126, 1996.
- 627 Dubuisson, P., Roger, J.C., Mallet, M., and Dubovik, O.: A code to compute the direct solar
628 radiative forcing: application to anthropogenic aerosols during the ESCOMPTE
629 experiment. In: Fischer, H. (Ed.), *Proceedings of the International Radiation Symposium:
630 Current Problems in Atmospheric Radiation*. A. Deepak Publishing, Busan, Korea, 2006.
- 631 Eck, T.F., Holben, B.N., Dubovik, O., Smirnov, A., Goloub, P., Chen, H.B., Chatenet, B., Gomes,
632 L., Zhang, X.Y., and Tsay, S.C. et al.: Columnar aerosol optical properties at AERONET
633 sites in central eastern Asia and aerosol transport to the tropical Mid-Pacific, *J. Geophys.
634 Res.*, 110, 2005.
- 635 Eck, T.F., Holben, B.N., Reid, J.S., Giles, D.M., Rivas, M.A., Singh, R.P., Tripathi, S.N.,



- 636 Bruegge, C.J., Platnick, S., Arnold, G.T., Krotkov, N.A., Carn, S.A., Sinyuk, A., Dubovik, O.,
637 Arola, A., Schafer, J.S., Artaxo, P., Smirnov, A., Chen, H. and Goloub, P.: Fog- and
638 Cloudinduced Aerosol Modification Observed by the Aerosol Robotic Network
639 (AERONET), *J. Geophys. Res.*, 117, 2012. D07206, doi: 10.1029/2011JD016839.
- 640 Eck, T. F., Holben, B. N., Sinyuk, A., Pinker, R. T., Goloub, P., Chen, H., Chatenet, B., Li, Z.,
641 Singh, R. P., and Tripathi, S. N.: Climatological aspects of the optical properties of
642 fine/coarse mode aerosol mixtures, *Journal of Geophysical Research: Atmospheres*
643 (1984–2012), 115, 19205, 2010.
- 644 Estellés, V., Campanelli, M., Utrillas, M. P., Expósito, F., and Martínezlozano, J. A.:
645 Comparison of AERONET and SKYRAD4.2 inversion products retrieved from a Cimel
646 CE318 sunphotometer, *Atmospheric Measurement Techniques*, 4, 569-579, 2012.
- 647 Fu, Q., Zhuang, G., Wang, J., Xu, C., Huang, K., Li, J., Hou, B., Lu, T., and Streets, D. G.:
648 Mechanism of formation of the heaviest pollution episode ever recorded in the Yangtze
649 River Delta, China, *Atmospheric Environment*, 42, 2023-2036, 2008.
- 650 García, O. E., Díaz, J. P., Expósito, F. J., Díaz, A. M., Dubovik, O., and Derimian, Y.: Aerosol
651 Radiative Forcing: AERONET Based Estimates, *Climate Models*, edited by: Druyan, L.,
652 ISBN: 978-953-51-0135-2, InTech, 2012.
- 653 Giles, D. M., Holben, B. N., Tripathi, S. N., Eck, T. F., Newcomb, W. W., Slutsker, I., Dickerson,
654 R. R., Thompson, A. M., Mattoo, S., and Wang, S. H.: Aerosol properties over the
655 Indo-Gangetic Plain: A mesoscale perspective from the TIGERZ experiment, *Journal of*
656 *Geophysical Research Atmospheres*, 116, 10--1029, 2011.
- 657 Giles, D. M., Holben, B. N., Eck, T. F., Sinyuk, A., Smirnov, A., Slutsker, I., Dickerson, R. R.,
658 Thompson, A. M., and Schafer, J. S.: An analysis of AERONET aerosol absorption
659 properties and classifications representative of aerosol source regions, *Journal of*
660 *Geophysical Research Atmospheres*, 117, 127-135, 2012.
- 661 Gobbi, G. P., Kaufman, Y. J., Koren, I., and Eck, T. F.: Classification of aerosol properties
662 derived from AERONET direct sun data, *Atmospheric Chemistry & Physics*, 6, 8713-8726,
663 2007.
- 664 Goloub, P., Li, Z., Dubovik, O., Blarel, L., Podvin, T., Jankowiak, I., Lecoq, R., Deroo, C.,
665 Chatenet, B., and Morel, J. P.: PHOTONS/AERONET sunphotometer network overview:



- 666 description, activities, results, Fourteenth International Symposium on Atmospheric and
667 Ocean Optics/Atmospheric Physics, 69360V-69360V-69315, 2007.
- 668 Gong, S.L., Zhang, X.Y., Zhao, T.L., Mckendry, I.G., Jaffe, D.A., and Lu, N.M.: Characterization
669 of soil dust aerosol in China and its transport/distribution during 2001 ACEAsia, 2. Model
670 simulation and validation, *J. Geophys. Res.*, 108, 4262. <http://dx.doi.org/10.1029/2002JD002633>, 2003.
- 671
- 672 Gyawali, M., Arnott, W. P., Lewis, K., and Moosmüller, H.: In situ aerosol optics in Reno, NV,
673 USA during and after the summer 2008 California wildfires and the influence of absorbing
674 and non-absorbing organic coatings on spectral light absorption, *Atmospheric Chemistry
675 & Physics*, 9, 8007-8015, 2009.
- 676 Hansen, J., Sato, M., Ruedy, R., Lacis, A., and Oinas, V.: Global warming in the twenty-first
677 century: an alternative scenario, *Proceedings of the National Academy of Sciences of the
678 United States of America*, 97, 9875-9880, 2000.
- 679 He, Q., Li, C., Geng, F., Yang, H., Li, P., Li, T., Liu, D., and Pei, Z.: Aerosol optical properties
680 retrieved from Sun photometer measurements over Shanghai, China, *Journal of
681 Geophysical Research Atmospheres*, 117, 81-81, 2012.
- 682 Holben, B. N., Eck, T. F., Slutsker, I., Tanré, D., Buis, J. P., Setzer, A., Vermote, E., Reagan, J.
683 A., Kaufman, Y. J., Nakajima, T., Lavenu, F., Jankowiak, I., and Smirnov, A.:
684 AERONET—A Federated Instrument Network and Data Archive for Aerosol
685 Characterization, *Remote Sensing of Environment*, 66, 1-16,
686 [https://doi.org/10.1016/S0034-4257\(98\)00031-5](https://doi.org/10.1016/S0034-4257(98)00031-5), 1998.
- 687 Holben, B. N., Tanré, D., Smirnov, A., Eck, T. F., Slutsker, I., Abuhassan, N., Newcomb, W. W.,
688 Schafer, J. S., Chatenet, B., and Lavenu, F.: An emerging ground-based aerosol
689 climatology: Aerosol optical depth from AERONET, *Journal of Geophysical Research
690 Atmospheres*, 106, 12067–12097, 2001.
- 691 Holben, B. N., Kim, J., Sano, I., Mukai, S., Eck, T. F., Giles, D. M., Schafer, J. S., Sinyuk, A.,
692 Slutsker, I., Smirnov, A., Sorokin, M., Anderson, B. E., Che, H., Choi, M., Crawford, J. E.,
693 Ferrare, R. A., Garay, M. J., Jeong, U., Kim, M., Kim, W., Knox, N., Li, Z., Lim, H. S., Liu,
694 Y., Maring, H., Nakata, M., Pickering, K. E., Piketh, S., Redemenn, J., Reid, J. S., Salinas,
695 S., Seo, S., Tan, F., Tripathi, S. N., Toon, O. B., and Xiao, Q.: An overview of meso-scale



- 696 aerosol processes, comparison and validation studies from DRAGON networks, Atmos.
697 Chem. Phys. Discuss., <https://doi.org/10.5194/acp-2016-1182>, in review, 2017.
- 698 Huang, X., Ding, A., Liu, L., Liu, Q., Ding, K., Niu, X., Nie, W., Xu, Z., Chi, X., Wang, M., Sun, J.,
699 Guo, W., and Fu, C.: Effects of aerosol–radiation interaction on precipitation during
700 biomass-burning season in East China, Atmos. Chem. Phys., 16, 10063-10082,
701 doi:10.5194/acp-16-10063-2016, 2016.
- 702 Hsu, N. C., Jeong, M. J., Bettenhausen, C., Sayer, A. M., Hansell, R., Seftor, C. S., Huang, J.,
703 and Tsay, S. C.: Enhanced Deep Blue aerosol retrieval algorithm: The second generation,
704 Journal of Geophysical Research-atmospheres, 118, 9296-9315, 2013.
- 705 Ichoku, C., Chu, D. A., Mattoo, S., Kaufman, Y. J., Remer, L. A., Tanré, D., Slutsker, I., and
706 Holben, B. N.: A spatio - temporal approach for global validation and analysis of MODIS
707 aerosol products, Geophysical Research Letters, 29, MOD1-1–MOD1-4, 2002.
- 708 Intergovernmental Panel on Climate Change (IPCC). Climate Change 2013. The Scientific
709 Basis; Cambridge University Press: New York, NY, USA, 2013.
- 710 Kaufman, Y. J., Tanré, D., and Boucher, O. A.: satellite view of aerosols in the climate system,
711 nature, 419, 215–223, 2002.
- 712 Kaufman, Y.J., Tanré, D., Remer, L.A., Vermote, E., Chu, A., and Holben, B.N.: Operational
713 remote sensing of tropospheric aerosol over land from EOS moderate resolution imaging
714 spectroradiometer, J. Geophys. Res., 102, 17051-17067, 1997.
- 715 Kong, S.F., Ji, Y.Q., Lu, B., Chen, L., Han, B., Li, Z.Y., and Bai, Z.P.: Characterization of PM10
716 source profiles for fugitive dust in Fushun—a city famous for coal, Atmos. Environ., 45,
717 5351–5365, 2011.
- 718 Lack, D. A., and Cappa, C. D.: Impact of brown and clear carbon on light absorption
719 enhancement, single scatter albedo and absorption wavelength dependence of black
720 carbon, Atmos. Chem. Phys., 10(9), 4207-4220, 2010.
- 721 Lee, K. H., Li, Z., Cribb, M. C., Liu, J., Wang, L., Zheng, Y., Xia, X., Chen, H., and Li, B.:
722 Aerosol optical depth measurements in eastern China and a new calibration method, J.
723 Geophys. Res., 115, 4038-4044, doi: 10.1029/2009JD012812, 2010.
- 724 Levy, R.C., Remer, L.A., Kleidman, R.G., Mattoo, S., Ichoku, C., Kahn, R., and Eck, T.F.:
725 Global evaluation of the collection 5 MODIS dark-target aerosol products over land,



- 726 Atmos. Chem. Phys., 10, 10399–10420, 2010.
- 727 Levy, R. C., S. Mattoo, L. A. Munchak, L. A. Remer, A. M. Sayer, F. Patadia, and Hsu, N. C.:
- 728 The Collection 6 MODIS aerosol products over land and ocean, Atmos. Meas. Tech.,
- 729 6(11), 2989–3034, 2013.
- 730 Li S., Wang T., Xie M., Han Y., and Zhuang B.: Observed aerosol optical depth and angstrom
- 731 exponent in urban area of Nanjing, China, Atmos. Environ., 123, 350–356, 2015.
- 732 Li, W.J., Shao, L.Y., and Buseck, P.R.: Haze types in Beijing and the influence of
- 733 agricultural biomass burning, Atmos. Chem. Phys. 10, 8119–8130, 2010.
- 734 Li, W., Li, P., Sun, G., Zhou, S., Yuan, Q. and Wang, W.: Cloud Residues and Interstitial
- 735 Aerosols from Non-precipitating Clouds over an Industrial and Urban Area in Northern
- 736 China, Atmos. Environ., 45, 2488–2495, doi: 10.1016/j.atmosenv.2011.02.044, 2011.
- 737 Li, W.J., Sun, J.X., Xu, L., Shi, Z.B., Riemer, N., Sun, Y.L., Fu, P.Q., Zhang, J.C., Lin, Y.T.,
- 738 Wang, X.F., Shao, L.Y., Chen, J.M., Zhang, X.Y., Wang, Z. F. and Wang, W.X.: A
- 739 conceptual framework for mixing structures in individual aerosol particles, J. Geophys.
- 740 Res., 121, 13205–13798, doi:10.1002/2016JD025252, 2016.
- 741 Li, Z., Niu, F., Lee, K., and Xin, J.: Validation and understanding of moderate resolution
- 742 imaging spectroradiometer aerosol products (C5) using ground-based measurements
- 743 from the handheld sun photometer network in China, J. Geophys. Res., 112,1–6, 2007.
- 744 Li, Z.Q., Eck, T., Zhang, Y., Zhang, Y.H., Li, D.H., Li, L., Xu, H., Hou, W.Z., Lv, Y., Goloub, P.
- 745 and Gu, X.F.: Observations of Residual Submicron Fine Aerosol Particles Related to
- 746 Cloud and Fog Processing during a Major Pollution Event in Beijing, Atmos. Environ., 86,
- 747 187–192, 2014.
- 748 Li Z., Lau, W.K.-M., Ramanathan, V., Wu, G., Ding, Y., Manoj, M.G., Liu, J., Qian, Y., Li, J.,
- 749 Zhou, T., Fan, J., Rosenfeld, D., Ming, Y., Wang, Y., Huang, J., Wang, B., Xu, X., Lee,
- 750 S.-S., Cribb, M., Zhang, F., Yang, X., Takemura, Wang, K., Xia, X., Yin, Y., Zhang, H., Guo,
- 751 J., Zhai, P.M., Sugimoto, N., Babu, S. S., and Brasseur, G.P.: Aerosol and Monsoon
- 752 Climate Interactions over Asia, Rev. Geophys., doi:10.1002/2015RG000500, 2016.
- 753 Liu, Q., Ding, W.D., Xie, L., Zhang, J.Q., Zhu, J., Xia, X.A., Liu, D.Y., Yuan, R.M., and Fu, Y.F.:
- 754 Aerosol properties over an urban site in central East China derived from ground
- 755 sun-photometer measurements, Science China Earth Sciences, 60, 297–314,doi:



- 756 10.1007/s11430-016-0104-3, 2017.
- 757 Lyapustin, A., Wang, Y., Xiong, X., Meister, G., Platnick, S., Levy, R., Franz, B., Korkin, S.,
758 Hilker, T., Tucker, J., Hall, F., Sellers, P., Wu, A., and Angal, A.: Scientific impact of MODIS
759 C5 calibration degradation and C6+ improvements, *Atmos. Meas. Tech.*, 7(12), 4353–
760 4365, 2014.
- 761 Mishra, A.K., and Shibata, T.: Synergistic analyses of optical and microphysical properties of
762 agricultural crop residue burning aerosols over the Indo-Gangetic Basin (IGB), *Atmos.*
763 *Environ.*, 57, 205–218, 2012.
- 764 Myhre, G.: Consistency between satellite-derived and modeled estimates of the direct aerosol
765 effect, *Science*, 325, 187–190, 2009
- 766 Pan, L., Che, H., Geng, F., Xia, X., Wang, Y., Zhu, C., Chen, M., Gao, W., and Guo, J.: Aerosol
767 optical properties based on ground measurements over the Chinese Yangtze Delta
768 Region, *Atmos. Environ.*, 44(21), 2587-2596, 2010.
- 769 Panicker, A.S., Lee, D.I., Kumkar, Y.V., Kim, D., Maki, M., Uyeda, H.: Decadal climatological
770 trends of aerosol optical parameters over three different environments in South Korea., *Int.*
771 *J. Climatol.*, 33, 1909–1916, 2013.
- 772 Pappalardo, G., Amodeo, A., Apituley, A., Comeron, A., Freudenthaler, V., Linné, H., Ansmann,
773 A., Bösenberg, J., D'Amico, G., Mattis, I. Mona, L., Wandinger, U., Amiridis, V.,
774 Alados-Arboledas, L., Nicolae, D., and Wiegner, W.: EARLINET: Towards an advanced
775 sustainable European aerosol Lidar network, *Atmos. Meas. Tech.*, 7, 2389–2409, 2014.
- 776 Remer, L.A., Kaufman, Y.J., Tanre, D., Mattoo, S., Chu, D.A., Martins, J.V., Li, R.R., Ichoku, C.,
777 Levy, R.C., Kleidman, R.G., Eck, T.F., Vermote, E., and Holben, B.N.: The MODIS aerosol
778 algorithm, products and validation, *J. Atmos. Sci.*, 62, 947-973, 2005.
- 779 Roger, J.-C., Mallet, M., Dubuisson, P., Cachier, H., Vermote, E., Dubovik, O., and Despiou, S.:
780 A synergetic approach for estimating the local direct aerosol forcing: applications to an
781 urban zone during the ESCOMPTE experiment, *J. Geophys. Res.*, 111, D13208,
782 <http://dx.doi.org/10.1029/2005JD006361>, 2006.
- 783 Russell, P.B., Bergstrom, R.W., Shinozuka, Y., Clarke, A.D., DeCarlo, P.F., Jimenez, J.L.,
784 Livingston, J.M., Redemann, J., Dubovik, O., and Strawa, A.: Absorption Angstrom
785 Exponent in AERONET and related data as an indicator of aerosol composition,



- 786 Atmos.Chem. Phys., 10, 1155–1169, <http://dx.doi.org/10.5194/acp-10-1155-2010>, 2010.
- 787 Sanap, S.D., and Pandithurai, G.: Inter-annual variability of aerosols and its relationship with
788 regional climate over Indian subcontinent, *Int. J. Climatol.*, 35, 1041–1053,
789 <http://dx.doi.org/10.1002/joc.4037>, 2014.
- 790 Schnaiter, M., Gimmler, M., Llamas, I., Linke, C., Jäger, C., and Mutschke, H.: Strong spectral
791 dependence of light absorption by organic carbon particles formed by propane
792 combustion. *Atmos. Chem. Phys.* 6, 2981–2990, 2006.
- 793 Schwartz, S.E., and Andreae, M.O.: Uncertainty in climate change caused by aerosols,
794 *Science*, 272, 1121–1122, 1996.
- 795 Shen X. J., Sun, J. Y., Zhang, X. Y., Zhang, Y. M., Zhang L., Che, H. C., Ma, Q. L., Yu, X. M.,
796 Yue, Y. and Zhang, Y. W.: Characterization of submicron aerosols and effect on visibility
797 during a severe haze-fog episode in Yangtze River Delta, China, *Atmospheric
798 Environment*, 120, 307-316, 2015.
- 799 Smirnov, A., Holben, B.N., Eck, T.F., Dubovik, O., and Slutsker, I.: Cloud screening and quality
800 control algorithms for the AERONET data base, *Remote Sens. Environ.*, 73, 337–349,
801 2000.
- 802 Solomon, S., Qin, D., Manning, M., Chen, Z., Marquis, M., Averyt, K.B., Tignor, M., Miller, and
803 H.L.(Eds.): *Climate change 2007: the physical science basis.*, Contribution of Working
804 Group I to the Fourth Assessment Report of the Intergovernmental Panel on Climate
805 Change. Cambridge University Press, Cambridge, United Kingdom and New York, USA,
806 2007.
- 807 Soni, K., Singh, S., Bano, T., and Tanwar, R.S.: Variations in single scattering albedo and
808 Angström absorption exponent during different seasons at Delhi, India. *Atmos. Environ.*,
809 44, 4355-4363, 2010.
- 810 Takamura, T., and Nakajima, T.: Overview of SKYNET and its activities, *Opt. Puray. Apl.*, 37,
811 3303–3308, 2004.
- 812 Tan, H., Wu, D., Deng, X., Bi, X., Li, F., and Deng, T.: Observation of aerosol optical depth over
813 the Pearl River Delta, *Acta Scientiae Circumstantiae.*, 29, 1146–1155, 2009 (in Chinese).
- 814 Tanré, D., Kaufman, Y.J., Herman, M., and Mattoo, S.: Remote sensing of aerosol properties
815 over oceans using the MODIS/EOS spectral radiance, *Journal of Geophysical Research.*,



- 816 102, 16971-16988, 1997.
- 817 Tao, M., Chen, L., Wang, Z., Tao, J., Che, H., Wang, X., and Wang Y.: Comparison and
818 evaluation of the MODIS Collection 6 aerosol data in China, *J. Geophys. Res. Atmos.*,
819 120, 6992–7005, doi:10.1002/2015JD023360, 2015.
- 820 Twomey, S.A., Piepgrass, M., and Wolfe, T.L.: An assessment of the impact of pollution on the
821 global cloud Albedo, *Tellus.*, 36B, 356-366, 1984.
- 822 Wang, L.C., Gong, W., Xia, X.A., Zhu, J., Li, J., and Zhu, Z.M.: Long-term observations of
823 aerosol optical properties at Wuhan, an urban site in Central China, *Atmos. Environ.*, 101,
824 94–102, 2015.
- 825 Wang, L.L., Xin, J., Wang, Y., Li, Z., Wang, P., Liu, G., and Wen, T.: Validation of MODIS
826 aerosol products by CSHNET over China, *Chinese Science Bulletin* 52 (12), 1708-1718,
827 2007.
- 828 Wang, P., Che, H.Z., Zhang, X.C., Song, Q.L., Wang, Y.Q., Zhang, Z.H., Dai, X., and Yu, D.J.:
829 Aerosol optical properties of regional background atmosphere in Northeast China, *Atmos.*
830 *Environ.*, 44, 4404–4412, 2010.
- 831 Wang, Z., Liu, D., Wang, Y., Wang, Z., and Shi, G.: Diurnal aerosol variations do affect daily
832 averaged radiative forcing under heavy aerosol loading observed in Hefei, China, *Atmos.*
833 *Meas. Tech.*, 8, 2901, 2015.
- 834 Wehrl, C.: Calibration of filter radiometers for the GAW Aerosol Optical Depth network at
835 Jungfraujoch and Mauna Loa. In: *Proceedings of ARJ Workshop, SANW Congress,*
836 *Davos, Switzerland*, pp. 70-71, 2002.
- 837 Wu, L.X., Lü, X., Qin, K., Bai, Y., Li, J.L., Ren, C.B., and Zhang, Y.Y.: Analysis to Xuzhou
838 aerosol optical characteristics with ground-based measurements by sun photometer (in
839 Chinese), *Chin Sci Bull*, 61: 2287–2298, doi: 10.1360/N972015-00874, 2016.
- 840 Xia, X., Chen, H., Goloub, P., Zong, X., Zhang, W., and Wang, P.: Climatological aspects of
841 aerosol optical properties in North China Plain based on ground and satellite
842 remote-sensing data, *J. Quant. Spectrosc. Radiat. Transf.*, 127, 12–23, 2013.
- 843 Xia, X., Li, Z., Holben, B., Wang, P., Eck, T., Chen, H., Cribb, M., and Zhao, Y.: Aerosol
844 optical properties and radiative effects in the Yangtze Delta region of China, *J. Geophys.*
845 *Res.*, 112, D22S12, doi:10.1029/2007JD008859, 2007.



- 846 Xiao, Q., Zhang, H., Choi, M., Li, S., Kondragunta, S., Kim, J., Holben, B., Levy, R. C., and Liu,
847 Y.: Evaluation of VIIRS, GOCI, and MODIS Collection 6 AOD retrievals against ground
848 sunphotometer observations over East Asia, *Atmos. Chem. Phys.*, 16, 1255-1269,
849 doi:10.5194/acp-16-1255-2016, 2016.
- 850 Xie, Y., Zhang, Y., Xiong, X.X., Qu, J.J., and Che, H.Z.: Validation of MODIS aerosol optical
851 depth product over China using CARSNET measurements, *Atmos. Environ.*, 45,
852 5970-5978, 2011.
- 853 Xin, J., Wang, Y., Li, Z., Wang, P., Hao, W., Nordgren, B., Wang, S., Liu, G., Wang, L., Wen, T.,
854 Sun, Y., and Hu, B.: Aerosol optical depth (AOD) and angstrom exponent of aerosols
855 observed by the Chinese Sun Hazemeter Network from August 2004 to September 2005,
856 *J. Geophys. Res.*, 112 (D05203), 2007.
- 857 Xin, J.Y., Zhang, Q., Gong, C.S., Wang, Y.S., Du, W.P., and Zhao, Y.F.: Aerosol direct radiative
858 forcing over Shandong Peninsula in East Asia from 2004 to 2011, *Atmos. Ocean. Sci. Lett.*,
859 7, 74-79, 2014.
- 860 Yan, P., Pan, X.L., Tang, J., Zhou, X.J., Zhang, R.J., and Zeng, L.M.: Hygroscopic growth of
861 aerosol scattering coefficient: a comparative analysis between urban and suburban sites
862 at winter in Beijing, *Particuology*, 7, 52–60, 2009.
- 863 Yang, M., Howell, S.G., Zhuang, J., and Huebert, B.J.: Attribution of aerosol light absorption to
864 black carbon, brown carbon, and dust in China – interpretations of atmospheric
865 measurements during EAST-AIRE, *Atmos. Chem. Phys.*, 9, 2035–2050,
866 <http://www.atmos-chem-phys.net/9/2035/2009/>, doi:10.5194/acp-9-2035-2009, 2009.
- 867 Zhang, L., Sun, J. Y., Shen, X. J., Zhang, Y. M., Che, H., Ma, Q. L., Zhang, Y. W., Zhang, X. Y.,
868 and Ogren, J. A.: Observations of relative humidity effects on aerosol light scattering in the
869 Yangtze River Delta of China, *Atmos. Chem. Phys.*, 15, 8439-8454,
870 doi:10.5194/acp-15-8439-2015, 2015.
- 871 Zhang, Q., Streets, D., Carmichael, G., He, K., Huo, H., Kannari, A., Klimont, Z., Park, I.S.,
872 Reddy, S., Fu, J., Chen, D., Duan, L., Lei, Y., Wang, L., and Yao, Z.L.: Asian emissions in
873 2006 for the NASA INTEX-B mission, *Atmos. Chem. Phys.*, 9, 5131-5153,
874 doi:10.5194/acp-9-5131-2009, 2009.
- 875 Zhang, X., Wang, Y., Niu, T., Zhang, X., Gong, S., Zhang, Y., and Sun, J.: Atmospheric aerosol



876 compositions in China: spatial/temporal variability, chemical signature, regional haze
877 distribution and comparisons with global aerosols. Atmos. Chem. Phys., 12, 779–799,
878 <http://dx.doi.org/10.5194/acp-12-779-2012>, 2012.

879 Zhao, H., Che, H., Ma, Y., Xia, X., Wang, Y., Wang, P, and Wu, X.: Temporal variability of the
880 visibility, particulate matter mass concentration and aerosol optical properties over an
881 urban site in Northeast China. Atmos. Res., 166, 204-212, 2015.

882 Zhao, H., Che, H., Zhang, X., Ma, Y., Wang, Y., Wang, X., Liu, C., Hou, B., and Che, H.:
883 Aerosol optical properties over urban and industrial region of Northeast China by using
884 ground-based sun-photometer measurement. Atmos. Environ., 75, 270–278, 2013.

885 Zhu, J., Che, H., Xia, X., Chen, H.B, Goloub, P., and Zhang, W.: Column-integrated aerosol
886 optical and physical properties at a regional background atmosphere in North China Plain.
887 Atmos. Environ., 84,54–64, 2014.

888 Zhuang, B., Wang, T., Li, S., Liu, J., Talbot, R., Mao, H., Yang, X., Fu, C., Yin, C., Zhu, J., Che,
889 H., and Zhang, X.: Optical properties and radiative forcing of urban aerosols in Nanjing
890 over China. Atmos. Environ., 83, 43–52, 2014.

891

892